Encoding of Sensory Signals Through Balanced Ionotropic Receptor Dynamics and Voltage Dependent Membrane Noise

Curtis Michel Marcoux

Neuroscience Program
Department of Cellular and Molecular Medicine
University of Ottawa

March 7th, 2016

Thesis submitted to the
Faculty of Graduate and Postdoctoral Studies
in partial fulfillment of the requirements
for the M.Sc. program in Neuroscience

Table of Contents

List of Figures Page number

Legend

ACSF	artificial cerebrospinal fluid
AMPA	alpha-amino-3-hydroxy-5-methyl-4-isoxazolepropionic acid
AM	amplitude modulation
APV	2-amino-5-phosphonopentanoic acid
cm	centimeter
CLS	centrolateral segment
CMS	centromedial segment
CNQX	6-cyano-7-nitroquinoxaline-2,3-dione
DCN	dorsal cochlear nucleus
DML	dorsal molecular layer
EA	electroreceptor afferents
EGp	eminentia granularis posterior
ELL	electrosensory lateral line lobe
EOD	electric organ discharge
EPSP	excitatory post synaptic potential
GABA	gamma-aminobutyric acid
GC	granule cell
Hz	hertz, per second
IBpI	interblip interval
IPSP	inhibitory post synaptic potential
ISI	interspike interval
LGN	lateral geniculate nucleus

LS	lateral segment
mm^2	square millimeters
mM	micromolar
ms	millisecond
mV	milliVolt
Na^+	sodium ion
NMDA	N-methyl-D-aspartic acid
NaP	persistent sodium
nP	nucleus praeminentialis
PCL	pyramidal cell layer
Pd	praeminentialis dorsalis
PTX	picrotoxin
RAM	random amplitude modulation
RF	receptive field
s	second
SC	serial correlation
SD	standard deviation
SR	stochastic resonance
V	volt
Var	variance
VCN	ventral cochlear nucleus
VML	ventral molecular layer
μm	micrometer

μS	microsiemens
μV	microVolt

Abstract

Encoding behaviorally relevant stimuli in a noisy background is critical for animals to survive in their natural environment. We identify core biophysical and synaptic mechanisms that permit the encoding of low frequency signals in pyramidal neurons of the weakly electric fish *Apteronotus leptorhynchus*, an animal that can accurately encode miniscule (0.1%) amplitude modulations of its self-generated electric field. We demonstrate that slow NMDA-R mediated EPSPs are able to summate over many interspike intervals of the primary electrosensory afferents (EAs), effectively eliminating the EA spike train serial correlations from the pyramidal cell input. This permits stimulus-evoked changes in EA spiking to be transmitted efficiently to downstream ELL pyramidal cells, where a dynamic balance of NMDA-R and GABA-A-R currents is critical for encoding low frequency signals. Interestingly, AMPA-R activity is depressed and plays a negligible role in the generation of action potentials; instead, cell intrinsic membrane noise implements voltage-dependent stochastic resonance to amplify weak sensory input and appears to drive a significant proportion of pyramidal cell spikes. Together, these mechanisms may be sufficient for the ELL to encode signals near the threshold of behavioral detection.

Acknowledgements

I would like to express my deep gratitude to Dr. Leonard Maler for his enthusiastic encouragement, creative suggestions and exemplary supervision over the past several years. It is through his guidance that I have been able to develop the critical reasoning skills necessary for a career in academia. His passion for neuroscience truly inspired me throughout my studies.

I would like to thank Dr. André Longtin for his advice and constructive recommendations. I thank Stephen Clarke, James Jun, Benjamin Elliott, Will Nesse, and Erik Harvey-Girard for stimulating discussions, insightful comments, and valuable suggestions throughout my project. I also wish to thank Bill Ellis for his valuable technical support throughout this project.

I am particularly grateful for the continuous love and support of my parents and brothers. Finally, I wish to thank Jenna Stirling for her patience and support throughout my study. Without her, this thesis would have not been possible.

Statement of Contributions

The collaborators listed in the submitted manuscript "Marcoux CM, Clarke SE, Nesse WH, Longtin A, Maler L, Balanced ionotropic receptor dynamics support signal estimation via voltage-dependent membrane noise" were Stephen Clark, Dr. Will Nesse, Dr. Andre Longtin, and Dr. Leonard Maler. Stephen Clark performed the in vivo experiments included in the manuscript, as well as contributed to the writing of software for data analysis. Dr. Will Nesse wrote software for the data analysis. Dr. Andre Longtin performed computational analyses and aided in revisions of the manuscript. Dr. Leonard Maler provided guidance and direction throughout the project, in addition to helping with revisions of the manuscript. All of the *in vitro* experiments and analysis, and writing presented here were done by the author.

Chapter 1: Introduction

1. Weakly Electric Fish

1.1 The Weakly Electric Fish as a Model Organism

Many factors must be taken into account in choosing a model organism for scientific study. Factors to be evaluated include, but are not limited to, the following: biological considerations, which include similarity to other organisms and suitability for intended study; practical considerations such as cost, space requirements and care needs; and historical considerations, which include the current extent of knowledge on the organism and specific tools or techniques that have been developed to study the organism.

The objective of our study was to examine the encoding and processing of the information contained in weak sensory signals. Consequently, we chose the weakly electric fish *Apteronotus leptorhynchus.* The weakly electric fish is a particularly well-suited model organism for the investigation of receptor dynamics in low-level sensory systems. Electrosensory signals are relatively simple and can be measured and mimicked with ease in a laboratory setting. The neural architecture of low-level electrosensory processing areas is relatively simple compared to the low level substrates of visual, acoustic and somatosensory processing in amniotes (e.g. mammals) and has been well characterized (Chacron et al., 2011; Marsat et al., 2012; Krahe and Maler, 2014; Clarke et al., 2015). Furthermore, techniques for both *in vivo* (Marsat et al., 2009) and *in vitro* (Maler, 1979; Harvey-Girard et al., 2010) studies of the weakly electric fish *A. leptorhynchus* have been described.

1.2 General Description of Weakly Electric Fish

Weakly electric fish are nocturnal organisms that are often found in turbid waters. Navigating through these murky waters is made possible by their electrosensory system that allow them to sense nearby objects, prey, and predators and to communicate with conspecifics. Weakly electric fish are distinguished from strongly electric fish (e.g. eels) in that the electric fields they produce are low in amplitude (~1 mV) and used for navigation, communication, and prey detection rather serve a direct offensive or defensive role. The ability to generate weakly electric fields is thought to have evolved independently in two groups of teleost fish, namely the South African Mormyriformes and the South American Gymnotiformes, and each group consists of hundreds of species (Bennett, 1971). The electric field can either be generated through a continuous and quasi-sinusoidal ("wave-type" species) electric organ discharge (EOD) or through a series of discrete and pulse-like EODs ("pulse-type" species). Wave EOD frequencies vary tremendously between species ranging from 50 Hz to around 1800 Hz. Pulse EODs are of considerably lower frequency, typically between 1 and 65 Hz at rest. The continuous production of an electric field in wave type species constantly consumes energy and as a result wave EOD are typically of lower amplitude than those of pulse type fish. My thesis focuses on the wave-type gymnotiform species, *Apteronotus leptorhynchus.*

1.3 Electric Organ

The EOD of an electric fish is generated from an electric organ of either myogenic or neurogenic origin. All of the mormyriforms and the gymnotiforms except

for the Apteronotid family possess myogenically derived electric organs (Kirschbaum, 1983). Myogenic electric organs consist of skeletal muscle derived electrocytes that are innervated by spinal motor neurons. The spinal motor neurons are controlled by a medullary pacemaker nucleus, which in turn is controlled by several pre-pacemaker nuclei located in higher brain centers (Markham, 2013). In contrast to the myogenically derived electric organ of all other weakly electric fish, that of the family *Apteronotidae* consists of the specialized terminals of spinal motor neurons. An important consequence of a neurogenic electric organ is that the use of a neuromuscular inhibitor to immobilize the fish does not silence the EOD, making the apteronotids particularly well suited for study. In both types of electric organ, electrocytes are stacked in series to increase voltage. This columnar arrangement of stacked cells, as well as the current and potential difference generated, is oriented rostro-caudally and generates a three dimensional electric field that surrounds the fish.

1.4 Electrosensory Stimuli

Apteronotus leptorhynchus are a wave-type species of weakly electric fish that emit a continuous high frequency EOD of 600 Hz to 1000 Hz, which permeates through their environment. The continuous electric field generated by the EOD is able to monitor the electrical impedance of the environmental surrounding the fish. The EOD is detected over the entire body of the fish as a transdermal potential difference. This potential difference is sensed by about 15,000 electroreceptor afferents, with approximately half the receptors located on head of the fish and the other half distributed over the trunk (Carr et al., 1982; Maler, 2009a). The density of electroreceptors is approximately 25 / mm^2 on the snout, 15 / mm^2 on the head, and 3 / mm^2 over the trunk (Carr et al., 1982). Objects

with electrical properties that differ from those of the surrounding water create distortions in the EOD that are represented as changes in the transdermal potential difference from baseline, and therefore alter current flow through epidermal electroreceptors on the skin surface. Each individual object projects a certain spatial pattern of current flow across surface electroreceptors that is referred to as an electric image. While electric images are very complex, there are two primary types of images that can be projected on to the skin surface: those from conductive objects and those from non-conductive objects. Conductive objects (e.g. prey) with impedance values below those of surrounding water will draw more electric current through them relative to the water that they are replacing. This in turn leads to a greater density of current entering the skin surface and an increase in the perceived EOD amplitude. In contrast, non-conducting objects (e.g. rocks) with impedance values higher than those of the surrounding water produce the opposite effect and therefore result in a reduction in the EOD amplitude.

1.5 Prey Capture

In addition to their specialized electrosensory system, weakly electric fish have a unique locomotor system allowing them to swim forward, backward, sideways and to hover in place, all while maintaining their trunk relatively rigid. These fish possess a long ribbon fin that extends along their ventral surface, and rippling of this fin allows for the wide range of movements previously described. The ability to independently control both their ribbon fin and trunk musculature minimizes EOD distortions due to movement. The versatility of movements allow weakly electric fish to exhibit complex behaviors during prey detection in order to optimize the quality and content of sensory information they acquire from their environment.

Fish of the family *Apteronotidae* are nocturnal predators that prey on small insect larvae and crustaceans in the freshwater lakes of South America. The fish swim with their head angled slightly downwards and lead with their dorsal edge; presumably, this strategy is a consequence of the higher density of electroreceptors on the dorsum of the fish and also to expose the head and trunk receptors to different volumes in order to increase sensory information. When prey has been detected, the fish will exhibit a reverse scan followed by a lunge to capture the prey (Lannoo and Lannoo, 1993; Nelson and Maciver, 1999). The reverse movement of the fish is accompanied by small shifts in posture that bring prey closer to the electrosensory skin surface causing a transdermal potential with a peak value normally in the range of several microvolts, however signals less than 1 microvolt can be detected. Mean prey detection distance is typically between 2 cm to 3 cm (Nelson and Maciver, 1999; Maciver et al., 2001). Integration times for sensory input expected during prey encounter is between 25 to 200 ms (Nelson and Maciver, 1999; Ratnam and Nelson, 2000). Together, the high degree of maneuverability and changes in body position, orientation, and velocity are behaviors that allow weakly electric fish to forage in complex environments and actively influence the spatiotemporal profile of sensory signals they encounter during prey-capture behavior.

1.6 Electroreceptors and Coding of Sensory Input

Two types of specialized electroreceptors transduce EOD distortions: time coding electroreceptors (T-units) and amplitude coding electroreceptors (P-units). T-units are phase locked to the EOD and fire one action potential per EOD cycle; as a result, the phase of the T-unit discharge with respect to the EOD is dependent on the local EOD intensity. Apteronotid T-units are only important for electrocommunication and their

central circuitry is separate from that of P-units; this thesis focuses on P-units, and T-units will not be further considered.

P-units are phase locked to the EOD, discharging in a probabilistic manner to the upstroke of the EOD oscillation (Nelson et al., 1997). P-units are composed of 25 to 40 receptor cells contained within a capsule below the skin surface and innervated by a single afferent axon, with each receptor cell making at least 16 synaptic contacts onto the axon (Bennett et al., 1989). Baseline P-unit discharge is not a random process, but shows negative interspike interval (ISI) serial correlations (SCs), where long ISIs are typically followed by shorter ISIs and vice versa (Ratnam and Nelson, 2000; Chacron et al., 2001; Gussin et al., 2007), and are a result of spike frequency adaptation (Benda et al., 2005). These negative correlations reduce low frequency noise levels and therefore reduce variability in the baseline discharge of P-units, thereby improving signal detection at low frequencies (Chacron et al., 2005).

The probability of a P-unit firing is proportional to the stimulus amplitude; consequently, P-unit firing rates carry information on amplitude modulations (AM) of the fishes' EOD. The spontaneous electroreceptor activity does not transmit information, but simply acts as a carrier for signals that are represented as distortions in amplitude. Baseline discharges of individual P-units are not correlated, with each P-unit independently coding sensory signals (Chacron et al., 2005). The probability of any given P-unit firing per EOD cycle is typically between 0.10 to 0.50 with a mean frequency of approximately 200 spikes/s (Gussin et al., 2007). The amplitude of the EOD can be modulated either by the EOD of conspecifics (electrocommunication) or by objects and prey with electrical impedance differing from that of the surrounding water

(electrolocation). Electrocommunication is typically associated with high frequency AMs that tend to range from 50 Hz to 500 Hz (Bastian and Nguyenkim, 2001), while prey signals are lower in frequency (<10 Hz) (Bastian and Courtright, 1991; Nelson and Maciver, 1999). P-units are able to transmit information with regard to EOD amplitude with great fidelity, with studies showing the proportion of the stimulus that can be linearly estimated from P-unit spike train to be as high as 80% of the AM (Wessel et al., 1996; Chacron, 2006).

1.7 Electrocommunication

In addition to electrolocation, weakly electric fish are able to use their combined electrogenic and electroreceptive capabilities for communication. In contrast to electrolocation, which produces local EOD distortions on the skin surface, communication signals are detected over a large extent of the body surface and are more readily detectable from greater distances away (Rasnow, 1996). Wave-type electric fish normally discharge at a fixed frequency, and when two electric fish are in close proximity their EODs overlap and produce a complex electric field. The difference in the frequency of the two EODs is referred to as the beat frequency, which can be readily discriminated by the fish. The electric fish can then modify their EOD in two behaviorally relevant ways: the jamming avoidance response or chirping. The jamming avoidance response (JAR) involves shifting the discharge frequency of each fish in order to increase the difference in EOD frequencies. The JAR is typically elicited by a beat frequency of less than 10 Hz (Heiligenberg, 1980) and serves to reduce the interference of beats on electrolocation (Matsubara and Heiligenberg, 1978). Weakly electric fish can also transiently (10 ms to 100 ms) increase their EOD frequency to produce active

electrocommunication signals termed chirps. Chirping behavior has been observed during courtship (Hagedorn and Heiligenberg, 1985), territorial encounters, and even when presented with laboratory mimics of conspecific's EOD (Engler and Zupanc, 2001)

2. ELL architecture

2.1 Multiple Electrosensory Maps

Electroreceptor afferents project sensory input directly from surface to the electrosensory lateral line lobe (ELL). The ELL is a laminar hindbrain structure that is divided into four adjacent segments. Ampullary receptors carry information with regards to exogenous low frequency signals and terminate in the medial segment (MS); these receptors will not be further discussed in my thesis. The three remaining maps receive sensory input exclusively from high frequency amplitude-coding tuberous receptors that trifurcate and project identical information to each of the centromedial (CMS), centrolateral (CLS) and lateral (LS) segments (Carr et al., 1982; Heiligenberg, 1991). Each map represents a somatotopic representation of the ipsilateral body surface. These three maps share similar morphology; however, there are no inter-map connections (Shumway, 1989) and each map demonstrates many distinct features and likely serve different roles. CMS pyramidal cells have a relatively small receptive field (RF), receiving input from approximately 25 electroreceptor afferents representing as little as 6 mm^2 of surface skin (Maler, 2009a). In contrast, pyramidal cells in the CLS receive converging input from around 100 afferents representing 26 mm^2, while those in the LS receive input from upwards of 600 afferents covering around 160 mm^2 of surface skin (Maler, 2009a). In addition to differences in RF size, CMS cells are tuned to lower frequencies compared those in the LS (Krahe et al., 2008). Finally, spontaneous

pyramidal cell spiking in the CMS and CLS are not phase locked to the EOD, while cells in the LS show significantly higher phase locking. As a result of map differences, pyramidal cells in the CMS likely respond preferentially to spatially localized low frequency signals (e.g. prey), while LS cells would preferentially respond to more diffuse high frequency signals (e.g. communication). CLS cells are intermediate in both RF size and tuning frequency. The observed differences of tuning frequency and RF size across maps, together with pyramidal cell type (discussed later), likely allow for parallel processing of sensory information.

Separate maps are a common finding in sensory systems (Young, 1998; Metzner, 1999). In most systems, sensory maps are repeated in both series and parallel at subcortical and cortical levels so that neurons that innervate adjacent sites in the sensory surface are also represented at adjacent sites in multiple central maps. For example, studies of the primate cerebral cortex have identified multiple parallel topographic representations of the retinal surface at several levels of processing that differ in their sensitivity to color, form, motion, object identification, and other aspects of visual stimuli (Felleman and Van Essen, 1991; Merigan and Maunsell, 1993). Additionally, studies of the mammalian auditory system have shown the existence of multiple separate pathways that begin at the level of the cochlear nucleus in the brainstem, each of which receiving the entirety of the cochlear frequency map (Young and Davis, 2002). These pathways project in parallel through the thalamus (Calford and Aitkin, 1983) and ultimately to several cortical auditory regions with different tuning properties (Rauschecker et al., 1997).

2.2 E and I cells

The laminar structure of the ELL is identical across all three topographic maps receiving tuberous receptor input. Electroreceptor afferents of tuberous receptors are located ventrally in the ELL and form the deep fiber layer (DFL) layer. These afferents then terminate more dorsally in the deep neuropil layer (DNL) (Maler, 1979; Maler et al., 1981) directly exciting the basilar dendrites of basilar (E-cells) pyramidal cells and indirectly inhibiting non-basilar pyramidal cells (I-cells) via granular cells. The granular cell nuclei form the granular cell layer (GCL), located just ventral and adjacent to the pyramidal cell layer (PCL). Morphologically, I-cells are distinguished from E-cells in that they lack a basal dendrite and therefore only receive sensory input indirectly. The indirect inhibition of I-cells occurs through an excitatory synapse between primary afferents and intermediate granular cell (GC) interneurons followed by an inhibitory connection between granular cells and I-cells. Excitatory potentials in the above mentioned synapses are primarily mediated through α-amino-3-hydroxy-5-methyl-4-isoxazolepropionic acid (AMPA) receptors and N-methyl-D-aspartate (NMDA) receptors, while the inhibitory connection between GC and I-cells is mediated by gamma-aminobutyric acid (GABA-A) receptors. As a result of this circuitry, a decrease in activity of electroreceptor afferents results in disinhibition, and therefore activation, of I-cells (Saunders and Bastian, 1984). As a consequence, E-cells and I-cells fire out of phase with one another, similar to retinal ON and OFF ganglion cells in vertebrates. Since E and I-cells have a receptive field (RF) of similar size (Bastian et al., 2002) and are found adjacent to one another within the PCL (Maler, 1979), they likely represent the same patch of skin on the surface of the fish. This implies that these fish have two separate topographic maps representing the same sensory surface within each of the maps

of the ELL (MS, CMS, CLS, LS), one for conductive objects (E-cells) and one for non-conductive objects (I-cells).

2.3 Columnar Organization

Within the PCL, E and I-cells can be further divided based on their dorsal-ventral position as superficial, intermediate, or deep cells, with each cell type showing both morphological and functional differences. These three categories of pyramidal cells were organized in a columnar fashion, with columns containing a superficial, intermediate, and deep pyramidal cell, as well as their non-basilar cell counterparts (Maler, 2009a). Measurements of basal dendrite overlap for each cell type within the column is near identical (Maler, 2009a), indicating that each cell within the column likely receives input from the same receptive field (Bastian and Courtright, 1991). In addition to their location within the PCL, superficial, intermediate, and deep pyramidal cells exhibit functional heterogeneity. In brief, superficial basilar pyramidal cells demonstrate stronger surround inhibition (Bastian et al., 2002), receive more feedback (Bastian et al., 2004), show phasic response patterns (Bastian and Courtright, 1991), and respond to sensory input in a more nonlinear manner (Chacron, 2006) when compared to deep pyramidal basilar neurons. These differences presumably result in better spatial and temporal resolution for superficial pyramidal cells and allow them to integrate and transform primary afferent input into complex non-linear signals. As a result of this organization, columns of pyramidal cells likely behave as the basic functional unit of the ELL, serving to optimize the encoding of complex sensory signals though the extraction of different information from the same primary afferent input (Marsat et al., 2009). This organization is similar to

the columnar arrangements of cells described in the mammalian neocortex (Mountcastle, 1997).

2.4 Feedback and Higher Brain Centers

Pyramidal cells are the only output cells of the ELL associated with the P-unit afferents, with projections to higher brain centers, most notably the midbrain torus semicircularis (TS) and the rhombencephalic nucleus praeminentialis dorsalis (Pd) (Berman and Maler, 1999). The TS functions primarily to integrate sensory information from the ELL and projects to higher brain centers for further processing (Carr et al., 1981). In contrast, the Pd is involved in two types of feedback pathways within the ELL: the direct and indirect feedback pathways. Direct feedback involves projections from Pd stellate cells via the stratum fibrosum (StF), located immediately dorsal to the PCL, terminating on the proximal apical dendrites of pyramidal cells in the ventral molecular layer (VML). Indirect feedback involves projections of Pd cells to a cerebellar structure - the eminentia granularis posterioris (EGp). EGp granule cells then project parallel fibers terminating in the dorsal molecular layer (DML), the dorsal most layer of the ELL, forming synapses at pyramidal cell apical dendritic spines. Notably, only deep pyramidal cells project to the nP, while TS receives input from all pyramidal cells types (Bastian et al., 2004). Both of these pathways are highly plastic and have been implicated in a number of complex functions, including cancellation of redundant signals (Bastian, 1996), network oscillations (Doiron et al., 2003), and enhancing the response to weak signals (Berman and Maler, 1999).

3. Thesis Objectives

The objective of my thesis is to examine the cellular and biophysical mechanisms that contribute to electrosensory signal encoding in the weekly electric fish *A. leptorhynchus*. The combination of easily characterized sensory input, reactively simple neural architecture, and well-described *in vivo* and *in vitro* electrophysiological techniques allows *A. leptorhynchus t*o serve an ideal model organism for the study of synaptic dynamics and their contribution to signal encoding. Through a series of electrophysiological experiments and computational analysis, I aim to systemically evaluate the contribution of various synaptic receptors to the encoding of prey like signals at the ELL electroreceptor afferent-pyramidal cell synapses. Furthermore, I evaluate the role of voltage-dependent membrane noise in amplifying these low frequency signals and ultimately evoking spiking in pyramidal cells.

Chapter 2 : Manuscript published in the Journal of Neurophysiology

Marcoux CM, Clarke SE, Nesse WH, Longtin A, Maler L (2016) Balanced ionotropic receptor dynamics support signal estimation via voltage-dependent membrane noise. *Journal of Neurophysiology*. 115, 530-545.

Introduction

Low-level sensory systems employ a balance of excitatory and inhibitory inputs to principal cells that, in turn, convey estimates of stimulus parameters (e.g. stimulus intensity) to higher level brain areas. The excitatory input may involve both AMPA and NMDA receptors, and the inhibitory input may involve both fast (GABA-A/glycine) and slow (GABA-B) channels. The effects of this specific balance of excitatory and inhibitory currents on stimulus encoding are currently unknown, as is the connection to the specific complement of receptor types. This scenario arises naturally in the electrosensory system of gymnotiform fish, animals which can encode a large range of stimulus intensities, extending down to barely detectable (Knudsen, 1974; Nelson and Maciver, 1999). We use the simplicity of electrosensory stimuli to show that the balance of excitatory (NMDA-R) and inhibitory (GABA-A) transmission, coupled with membrane noise, enables an accurate encoding of electrosensory signal amplitude.

Individual *Apteronotus leptorhynchus* emit a constant high frequency electric organ discharge (EOD, species range: ~700-1000 Hz). The EOD generates an electric field around the fish sensed by ~15,000 electroreceptors that drive electroreceptor afferents (EAs). The EOD drives EA discharge in a probabilistic manner with a mean frequency of 200 spikes/s (Gussin et al., 2007). Objects with conductivity greater (e.g. prey) or less (e.g. rocks) than the ambient water perturb the field to generate a spatially localized electric image – electrically "bright" or "dark" patches on the skin. Behavioral studies (Nelson and Maciver, 1999) have shown that the electrosense is essential for prey

capture. Detection can occur with prey further than 3 cm from the fish's body (Nelson and Maciver, 1999), which translates to a <1 μV increase over a baseline EOD amplitude of ~1.3 mV (Nelson and Maciver, 1999; Chen et al., 2005). In a prey detection time window of 200 ms, these ultra-weak stimuli cause the average EA to increase its discharge by ~1 spike relative to a baseline of 40 spikes (Bastian, 1981a; Nelson et al., 1997; Gussin et al., 2007).

Baseline EA discharge is not completely random but exhibits negative interspike interval (ISI) serial correlations (SCs) – i.e. a long ISI is followed by a shorter one and vice versa (Ratnam and Nelson, 2000; Chacron et al., 2001; Gussin et al., 2007). These SCs reduce EA spike count variability over the 200 ms detection window (Ratnam and Nelson, 2000; Chacron et al., 2001) and can therefore improve the fish's ability to encode prey signals via a rate or spike count code (Chacron et al., 2005). Detailed calculations suggest that, even with this reduction in variability, the small increase in spike count produced by the weakest prey signals is not sufficient for prey detection (Gussin et al., 2007; Maler, 2009b). Several more sophisticated detection models that utilize some form of temporal coding have been proposed. These theories all use stimulus-induced deviations from expected ISI correlations to improve signal encoding over the limits imposed by simple trial-based spike counts. The proposed mechanisms include temporal filtering plus integration of EA spike trains (Goense and Ratnam, 2003), or continuously computing conditional probabilities of successive ISIs via short-term plasticity (Ludtke and Nelson, 2006). It is, however, difficult to devise experimental tests of these theoretical mechanisms. Nesse et al. (2010) demonstrated that, in theory, an encoding/decoding mechanism that matched pre- and post-synaptic kinetics could utilize

the serial correlation between only two successive ISIs to encode weak signals. Our results below are a first step towards confirming this theory.

Glutamatergic EAs terminate in three topographic maps within the electrosensory lobe (ELL): the centromedial (CMS), centrolateral (CLS) and lateral (LS) segments (Krahe and Maler, 2014). The CMS and CLS are both strongly responsive to the spatially localized low-frequency signals associated with, e.g. prey, while the LS is more specialized for processing spatially diffuse electrocommunication signals (Krahe and Maler, 2014). In all maps the EAs drive two classes of output pyramidal neurons (Maler, 1979, 2009a; Krahe and Maler, 2014; Clarke et al., 2015) as illustrated in Figure 1. EAs terminate directly onto AMPA and NMDA receptor-rich ON-type pyramidal cells (previously described as E cells), and GABAergic interneurons (Bastian, 1981b; Maler et al., 1981; Maler and Mugnaini, 1994; Berman and Maler, 1998). These interneurons in turn inhibit the ON cells. ON cells typically detect conductive objects. OFF-type pyramidal cells (previously described as I cells) receive indirect EA input via the inhibitory interneurons and therefore typically respond to non-conductive objects (Bastian, 1981b; Maler et al., 1981; Maler and Mugnaini, 1994; Berman and Maler, 1998).

In this paper we use ELL slices to investigate the cellular mechanisms by which *A. leptorhynchus* can encode low-frequency prey signals. In order to get discernible synaptic responses in ON and OFF cells, we had to stimulate using pulse patterns derived from moderate to strong signals (>3 μV, see Methods). Our results directly pertain to the cellular mechanisms by which such signals are encoded in the firing rate of EAs; they do not, however, directly address the mechanisms by which the weakest signals are detected.

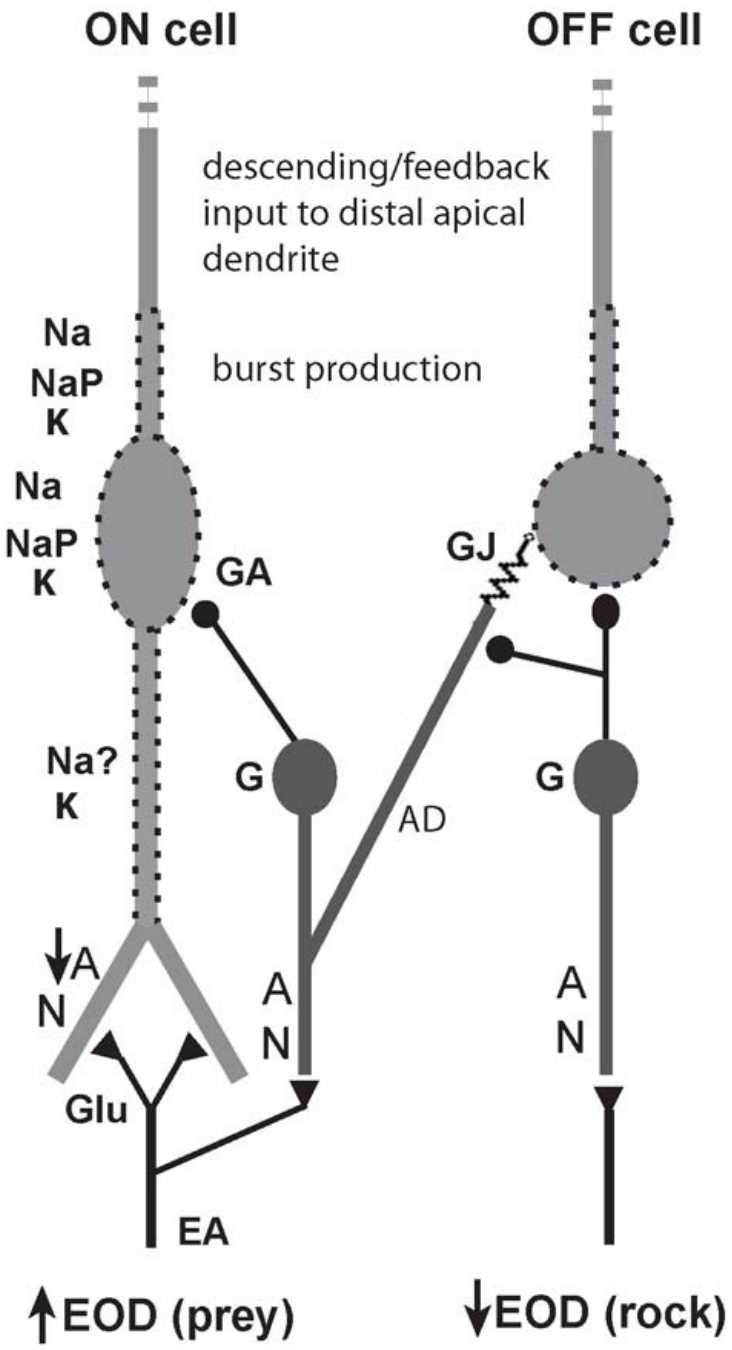
ON cell
OFF cell
descending/feedback input to distal apical dendrite
burst production
Na
NaP
K
Na
NaP
K
GA
GJ
Na?
K
G
G
AD
A
N
A
N
A
N
Glu
EA
EOD (prey)
EOD (rock)

Figure 1. Summary diagram of the ELL circuitry that generates the ON and OFF cell responses. ON cells receive direct glutamatergic (Glu) synaptic input from EA afferents onto their basal dendrites; glutamate excites the ON cell via AMPA (A) and NMDA (N) receptors. The AMPA component of the EA evoked EPSP shows strong short term depression (down arrow beside 'A'). The EAs also contact local GABAergic interneurons (G) that, in turn, synapse on the ON cell somata utilizing GABA-A receptors (GA). The net effect of this arrangement is that increases in EOD intensity within the receptive field of the ON cell due to a conductive object, e.g. prey, will depolarize the ON cell and elicit increased spiking. Immunocytochemistry and physiological studies have shown that the soma and proximal apical dendrite of the ON cell express both fast (Na) and persistent (NaP) Na^+ channels as well as K^+ (Kv3) channels. The basal dendrite of the ON cell also expresses Na^+ channels (immunocytochemistry) but it is not known whether these are the fast or persistent variety or both (therefore Na?). The OFF cell receives input from EAs only disynaptically via the same GABAergic interneuron; this inhibitory input generates the OFF cell receptive field center. Excitation of the OFF cell is via gap junction (GJ) input from ascending dendrites (AD) of the same interneurons; these, however, emanate from distant cells and therefore represent more distant body regions (receptive field surround). The GABAergic interneurons that inhibit the OFF cell also inhibit the ascending dendrites. The net effect of this circuitry is that a decrease in EOD intensity due to, e.g. a rock, will reduce the direct inhibition of the OFF cell and, via the ascending dendrite and gap junction synapses, also permit excitation from distant regions of the fish's skin. The OFF cell will therefore invert the electrosensory input and give a spiking response to non-conductive objects. The OFF cell also expresses the same Na^+ and K^+

channels as the ON cell. The circuitry illustrated in this figure was first demonstrated in Maler (1979) and Maler et al. (1981).

We focus on four specific questions of EA and ELL ON cell physiology: a) are EA negative ISI serial correlations transmitted to ON cells as negative SCs of evoked EPSP amplitudes? b) what are the respective roles of AMPA- and NMDA-R components of the EA-evoked ON cell EPSPs in transmitting information about local low-frequency signals (e.g. prey)? c) is the disynaptic GABA-A mediated inhibition of ON cells essential for transmitting such information, or does it serve to simply prevent saturation of the ON cell excitatory EA input? d) can membrane noise aid in signal encoding, or is it merely an unavoidable contamination that limits encoding of low-frequency signals? We now elaborate on these individual questions.

a) We have previously shown that the AMPA-R component of the EA to ON cell synapses exhibits short-term presynaptic depression with rapid recovery (Khanbabaie et al., 2010). As we discuss in detail below, this should lead to a negative SC of the AMPA-R peaks at each EA to ON cell synaptic contact. These correlations might, over a short time scale (<200 ms), interfere with the signal-induced modulations of synaptic release at this site, i.e. be a synaptic source of high-frequency noise. We hypothesize that the EA correlations are removed by postsynaptic dynamics and analyze this possibility in detail. As a second focus of this section, we note that the Nesse et al analysis (2010) shows that a matching of pre- and post-synaptic dynamics can eliminate the EA SCs. Although our data cannot prove this model, it could lend preliminary support to it; it could also disprove it if the SCs persist in the ON cell EPSP amplitudes.

b) In ELL slices, the AMPA-R component of the EA evoked EPSP (ON cell) can trigger spiking (Berman and Maler, 1998) suggesting that these receptors are important for signal encoding. This conclusion appears to be contradictory to the depression of the

AMPA-R component of the evoked EPSPs when EAs are driven above their baseline frequency (Khanbabaie et al., 2010). We hypothesize that the slow NMDA-R component of the evoked EPSP will then be critical for encoding slow signals (e.g. prey) and test this idea.

c) EAs contact local GABAergic interneurons and evoke disynaptic IPSPs in ON cells (Maler and Mugnaini, 1994; Berman and Maler, 1998). We consider two possible roles of this inhibition. First, it may merely prevent the high frequency excitatory EA input to the ON cells from saturating their response. Second, the disynaptic inhibition may be a critical component of signal encoding by ON cells. We address these hypotheses in two ways. First, we examine ON cell stimulus encoding in the absence of inhibition (pharmacological blockade). Second, we examine signal encoding in OFF cells. OFF cells are not directly contacted by EAs, but do receive disynaptic inhibition from the same GABAergic interneurons as ON cells. We therefore reason that, if OFF cells can encode low-frequency signals, it would support our second hypothesis: that inhibition is required for signal encoding in ON cells.

d) The first *in vitro* study of ELL reported that ON and OFF cells exhibited membrane noise (Mathieson and Maler, 1988). This noise was voltage-dependent and might therefore be expected to increase with stimulus-evoked excitation of ON cells. This noise might first appear to be counterproductive for signal encoding. We therefore studied this noise in greater detail and, specifically, tried to connect it to the EA-evoked ON cell depolarization. Our data led us to hypothesize that the membrane noise may drive ON cell spiking via the conversion of subthreshold smooth NMDA-R-dependent synaptic input into spike trains (Stacey and Durand, 2001). This is an ingredient of the

stochastic resonance (SR) signal enhancement effect (Longtin, 1993; McDonnell and Ward, 2011), here for low-frequency signals such as prey. Although it is not possible experimentally to vary noise levels alone to verify that SR is at play, our results show recruitment of noise near threshold, and thus point to noise-driven firing to assist the detection and encoding of stimuli. A major implication of our results on SR is that the responses of pyramidal cells with overlapping receptive fields should not be correlated, since their internal noise sources are likely independent. We explore this possibility in some detail (see Discussion).

Both the CMS and CLS are very sensitive to the electrosensory signals associated with prey (Krahe and Maler, 2014). Our *in vitro* analysis of how prey signal mimics are transmitted across the EA to ON cell synapses was, for technical reasons, confined to the CMS (see Methods). Our *in vivo* and *in vitro* analysis of the contribution of noise to stimulus amplification was, again for technical reasons, done mainly in the CLS (see Methods).

Methods

In vitro recordings

The weakly electric fish, *Apteronotus leptorhynchus* (male and female, 10 – 15 cm in length) was used in these studies. Adult fish of both sexes were deeply anaesthetized in oxygenated water with 0.2% 3-aminobenzoic ethyl ester (Tricaine Methanesufonate, MS-222; Sigma) and transverse slices were prepared as previously described (Harvey-Girard et al., 2010). In brief, fish were transferred to a foam-lined holder and their gills were superfused with water containing the anesthetic, whereupon the ELL was removed. The

ELL was then immersed in ice-cold artificial cerebrospinal fluid (ACSF; 124 mM NaCl, 3 mM KCl, 0.75 mM KH_2PO_4, 2 mM $CaCl_2$, 1.5 mM $MgSO_4$, 24 mM $NaHCO_3$, and 10 mM D-glucose) containing 1 mM kynurenic acid and transferred to a vibratome (Technical Products International, St. Louis, MO), where 350 um slices were taken from the transverse plane of the ELL (Maler, 1979). The ELL slices were transferred to an interface slice chamber with flowing oxygenated ACSF for a minimum of one hour at room temperature before recordings began.

Stimulation and Recording procedures

Intracellular recordings were obtained from pyramidal cells of the centromedial segment (CMS) of the ELL using sharp microelectrodes (80 – 120 MΩ). We used the CMS because EA afferent fibers to this map are confined to compact narrow bundles (Lannoo et al., 1989); we could usually place the bipolar stimulating electrodes over most of the extent of such bundles and thereby evoke strong, readily measured EPSPs. The greater dispersal of the EA afferent fibers in the CLS and LS maps made it far more difficult to find a stimulation site that evoked strong, consistent responses. We selected mainly ON-type pyramidal cells since they receive direct input from the EAs onto their basal dendrites and this greatly simplifies our analysis (Maler, 1979; Maler et al., 1981; Berman and Maler, 1998). We identified ON cells by stimulating the EA afferents: ON cells exhibit short latency EPSPs in response to such stimulation while OFF cells exhibit IPSPs (Berman and Maler, 1998; Harvey-Girard and Maler, 2013). In a few cases, in order to evaluate whether their inhibitory input contributed to stimulus encoding by ON cells, we also recorded from OFF cells that are in receipt of the GABA-A receptor mediated disynaptic inhibition from the same interneurons as the ON cells (Maler, 1979;

Maler et al., 1981; Maler and Mugnaini, 1994; Berman and Maler, 1998). For studies of synaptic transmission between the EAs and downstream pyramidal cells, all active conductances were blocked by routinely filling the pipettes with cesium acetate, lidocaine *N*-ethyl bromide (QX-314, 100 mM in 3 M CsAc, Alomone Labs, Jerusalem, Israel), and tetraethylammonium (TEA, 50 μ M, Sigma- Aldrich, St. Louis, MO) (Berman et al., 2001; Khanbabaie et al., 2010). As previously reported (Khanbabaie et al., 2010) cells stopped spiking in response to depolarizing current in < 5 minutes after impalement and experiments were commenced at this time. In this case, the ON cells effectively become passive reporters of the EA evoked synaptic potentials. In order to evaluate the role of NMDA-R in ON cell responses we bath applied 2-Amino-5-phosphonopentanoic acid (APV; 100 μ M, Tocris, Bristol, UK) to block the NMDA-R mediated components of the electroreceptor afferent evoked EPSP (Berman and Maler, 1998; Khanbabaie et al., 2010). We first recorded the control response and then applied APV, while delivering single EA stimulating pulses every few seconds. Once the late phase of the EPSP had completely disappeared (at least 10 minutes) we initiated our stimulus protocols. For the APV experiments we therefore always compare the same cell for control and blockade conditions. Given the long times required for these interventions, we were not able to hold the cells long enough for washout. In some cases, we also included picrotoxin (PTX, 100 μ M, Sigma- Aldrich, St. Louis, MO) in the recording pipette to block the disynaptic GABAergic input to all pyramidal cells. Again, we gave stimulating pulses to the EAs to determine when the evoked IPSP was fully blocked; as previously reported (Khanbabaie et al., 2010) the IPSP was eliminated in < 9 minutes and experiments were then initiated. In this case, we could not record a true control response to EA stimulation because

blockade was gradual.

Membrane potentials were recorded with an Axoclamp 900A (Molecular Devices, Sunnyvale, California) and the experiments were controlled with a Power 1401 data acquisition interface and associated Spike 2 software (Cambridge Electronic Design, Cambridge, UK). The voltage signal was amplified, low-pass filtered at 10 kHz, digitized at 20 kHz, and analyzed off-line using custom Matlab routines (MathWorks, Natick, Massachusetts). EPSP amplitude was defined as the difference in the average membrane potential just prior to the occurrence of the stimulus artefact and the subsequent EPSP maximum. EPSP latency was measured as the time delay between the occurrence of the artefact and the subsequent EPSP maximum.

Pulse stimulation of the EA fibers was accomplished with a gold tipped bipolar tungsten electrode, positioned in the deep fiber layer (DFL) of the ELL (Berman and Maler, 1998; Khanbabaie et al., 2010). The stimulus electrode was placed along the EA tract at least 300 μm from the recording site and the stimulus intensity was adjusted to prevent direct stimulation of the impaled pyramidal cells. The square wave pulse (20 μs, 1–80 V) stimulus was delivered through a signal isolation unit (model DS2, Digitimer, Welwyn Garden City, UK). Stimulus intensity (50 – 80 V) was set to evoke 70% of the maximal EPSP amplitude to facilitate the detection of the starting point of EPSPs with short latencies (~ 1 ms). Electroreceptor afferents run in a tight bundle to reach the CMS (Lannoo et al., 1989) and, since our bipolar stimulating electrode straddled the entire afferent tract, we likely stimulated a large fraction of the ~25 EAs that converge onto a single ON type pyramidal cell (Maler, 2009a). Peak EPSP values ranged from <1 mV to 9 mV with the highest value presumably representing stimulation of nearly all of the

innervating EAs. We only accepted cases where the evoked EPSP was greater than 0.5mV and we confirmed that the stimulus artefacts did not change during the course of a recording. Stimulus artefacts were removed from the membrane potential data offline using custom scripts in Matlab (MathWorks, Natick, Massachusetts). Using the known stimulus pulse sequence, artefact peaks were localized and the membrane potential was removed for at most 1 ms preceding, and 2 ms following the timing of the peak. Cubic spline interpolation was then used to replace the ≤ 3 ms of excised recorded membrane potential. The peaks of the evoked EPSPs were identified by locating a local maximum in the membrane potential between successive stimulus artefact peaks and starting 2 ms after the peak to avoid contamination with the interpolated membrane potential. The amplitude was then measured as the difference between the value of the membrane potential at the EPSP peak and the membrane potential 1 ms before the occurrence of the stimulus artefact that drove the EPSP; this is the last value of the membrane potential that occurs before the artefact contaminates the signal.

Two stimulation patterns were used in this study, both derived from *in vivo* recordings of electroreceptor afferent activity (Gussin et al., 2007). We chose electroreceptor afferent recordings with moderate mean frequencies of 115 spikes/s and 128 spikes/s because higher frequency EAs often produced very short inter-pulse intervals (IPIs<3 ms); in these cases, the stimulus artefact of the second pulse obscured the peak of the EPSP evoked by the first pulse.

We used both the baseline discharge and evoked responses of these EAs as stimuli. In the case of baseline discharge, the EAs are driven by the constant amplitude of the fish's electric organ discharge (EOD) and variation in the spike train IPIs are due

to the internal dynamics of the receptor and its afferent fiber. We also used pulse trains derived from one of the EA's spiking responses to 0-4 Hz random amplitude modulations (RAMs) of the fish's EOD (Gussin et al., 2007). Low-frequency amplitude modulations are typical of electrolocation, and are commonly experienced during navigation and prey capture (Nelson and Maciver, 1999). In order to average across recordings from many pyramidal cells, we used a single short stretch of stimulus lasting one second and included both strong (~ 80 μ V) and moderate (<5 μ V) amplitude modulations. In preliminary tests we found that stimulation for >2 s resulted in clear run down of the evoked EPSPs. We therefore chose to use a minimal stimulus duration of 1 s to avoid the artefactual reduction of EPSPs towards the end of the stimulus period. We compared the evoked pyramidal cell membrane potential fluctuations to the external sensory stimulus using a correlation measure as done in previous *in vivo* studies (Chacron et al., 2003; Bastian et al., 2004). Although these stimulus pulse patterns were derived from *in vivo* recordings of EAs, our stimulation method causes synchronous activation of all EAs, whereas *in vivo* such low-frequency stimuli would evoke increased but uncorrelated discharge across the EA population contributing to the receptive field of the recorded neuron (Benda et al., 2006; Maler, 2009a). This effect of this difference is analyzed further below.

To characterize the intrinsic pyramidal cell noise, we recorded ON cells from both the CMS and CLS maps (Krahe and Maler, 2014). The recording pipette was filled with 2 M potassium acetate only. In these cases we bath applied 6-cyano-7-nitroquinoxaline-2,3-dione (CNQX, 1mM, Tocris, Bristol, UK) and APV to block all synaptic input to pyramidal cells (Berman and Maler, 1998). We again used single EA stimulating pulses

and initiated recording when we could not record any synaptic response (at least 10 minutes). In these cases, we could not perform a control case because membrane fluctuations before complete synaptic blockade could result from either membrane or synaptic noise. After drug application, any remaining membrane fluctuations could then be attributed to cell-intrinsic sources. Studies examining the intrinsic membrane fluctuations (noise) of ELL pyramidal cells used two-second holding currents to maintain the impaled cell at various membrane potentials (see Results below). We started by applying sufficient holding current to bring the cell above spike threshold. For the cell in Fig. 6 spike threshold was at ~-65 mV, consistent with the pyramidal cell threshold in CMS (approximately -63 to -67 mV, (Mehaffey et al., 2008). For the illustrated cell we first depolarized by 5 mV to -60 mV (Fig. 6B) to induce strong membrane noise and robust spiking (Fig. 6A, B); in order to compare levels of depolarization (above spike threshold) across cells; this suprathreshold level of depolarization was set to 0 as in Fig. 6A. From the above threshold membrane potential, we then stepped the injected current so as to produce -5 mV hyperpolarizations, bringing the cell down to -20 mV below the initial holding potential. Therefore, different holding currents were used for each cell to preserve this relative relationship to spike threshold.

In vivo recordings

Fish were anesthetized and the caudal cerebellum, overlying the ELL, was exposed. After stopping general anesthesia, a local anesthetic was applied to the wound margins. Fish were immobilized with a size-dependent dose of pancuronium bromide, injected intramuscularly, and were respirated with a constant flow of aerated water for the duration of the experiment. The fish were transferred into a large tank of 27 °C water

with the electrical conductivity kept between 100-120 μS/cm, and a custom holder was used to stabilize the head during long-term recordings. Fish were given time to acclimatize before data acquisition and were monitored closely for signs of stress.

Single unit extracellular recordings were obtained from the CLS map of the ELL for direct comparison of pyramidal cell spiking to the *in vitro* data described above. One reason the CLS map was preferred for these studies is that the receptive fields of CLS pyramidal cells are much larger than those of CMS and therefore much easier to localize (Maler, 2009). Pyramidal cells with receptive fields near the fish's dorsum (at the water's edge) were excluded from the analysis due to their proximity to the air-water interface, where boundary effects warp the electric field. Once a suitable cell was located and its firing rate and type (ON or OFF) verified with local steps in the electric potential, long sections of baseline activity were recorded and used to compute ISI serial correlations. The serial ISI correlation coefficients for lag j (SC(j)) are defined as

$SC(j) = < \frac{< I_{i+j} I_j > - < I_j >^2}{Var(I)} >$ where <.> represents the average value and Var(I) the variance of the ISIs. An average serial correlation was determined for 5 ON and 5 ON cells from 3 different fish. Analysis was performed using custom Matlab scripts. All procedures were reviewed and approved by the Animal Care Committee at the University of Ottawa and follows Society for Neuroscience guidelines.

Results

Elimination of electroreceptor afferent inter-spike interval serial correlations by slow NMDA-R mediated EPSPs

It has previously been shown that the baseline activity of EAs exhibit a negative ISI correlation at lag 1, indicative of sensitivity to the timing of the last two action potentials (Ratnam and Nelson, 2000). The effect of synaptic transmission on such correlations has not been well studied. A theoretical analysis did demonstrate that pre-synaptic depression can suppress positive ISI correlations in incoming spike trains, resulting in much less correlated ISIs impacting the post-synaptic receptors (Goldman et al., 2002). Recent theoretical work has also shown that correlations in input currents (but not ISIs per se) can be transferred to output ISIs (Schwalger et al., 2015); but little is known about input to output transfer of ISI correlations. If an input spike strongly influences spiking probability, then one might intuitively expect that ISI correlations are transferred, but the situation is less clear when many spikes from different neurons are required to fire the cell, and when there is noise, which are both the situation of interest here. Our results below therefore advance on knowledge on ISI correlation transfer and also raise interesting questions in this context.

The baseline activity of target ELL pyramidal cells is effectively a renewal process with minimal or no ISI correlations (shown below in the *in vivo* section). The elimination of ISI correlations might be achieved at many levels of the ELL circuitry or via intrinsic properties of the pyramidal cells. In the absence of spiking and thus network feedback, our goal was to understand whether EA to CMS pyramidal cell synaptic dynamics can, by itself, remove the EA correlation structure. An earlier study established

that blocking AMPA-R mediated transmission with CNQX also blocks NMDA transmission (Berman et al., 1997). Therefore, we assume that AMPA transmission is crucial in sufficiently depolarizing pyramidal cell basal dendrites to unblock NMDA-R channels, and is required for transmitting electrosensory signals from EAs to pyramidal cells. For experiments examining the mechanisms of decorrelation and signal transmission, we consequently tested the role of NMDA and GABA-A receptors by first studying the intact system and then systematically eliminating the NMDA and GABA-A receptor components.

ELL ON cells receive direct electroreceptor afferent input onto their basal dendrites (Fig. 1) (Berman and Maler, 1998). With intrinsic conductances pharmacologically blocked (see Methods) but AMPA, NMDA and GABA receptors intact, stimulation of electroreceptor afferent with a natural baseline discharge pattern induced rapid summation of evoked potentials to a plateau level (Fig. 2A, left). This is consistent with a previous study showing that temporal summation results in a plateaued potential when using a 200 Hz stimulus train (Khanbabaie et al., 2010). Stimulating the EAs with these high-frequency stimulus trains evokes a complex sequence of IPSPs and EPSPs in the pyramidal cells, which vary greatly in amplitude (Fig. 2A, right). In some recordings it is possible to distinguish between the NMDA and AMPA-R components of the pyramidal cell EPSP (Fig. 2A). As previously shown (Berman and Maler, 1998; Khanbabaie et al., 2010), the AMPA-R component appears as a rapidly rising, short latency response that can decay before full activation of the NMDA-R, which has a longer latency and slower rate of rise. This produces a prominent “notch” in the evoked

EPSP. It is important to note that the magnitude of the fast AMPA-R component of the EPSP is always far smaller than the slower NMDA-R component.

Electroreceptor afferent evoked EPSPs vary in amplitude depending on the previous ISI length. After short ISIs, the NMDA-R component of the EPSPs summates and typically generates EPSPs with near equal or larger amplitudes (Fig. 2A, right). This result stands at odds with our previous study using fixed frequency or random stimulation (Khanbabaie et al., 2010) where, in the presence of NMDA and GABA-A receptor antagonists, strong and fast presynaptic depression of the EA-evoked EPSP was observed following short ISI stimulus pulses.

To resolve this issue, we repeated our earlier study by first blocking NMDA receptors alone with APV. We note that this drug application does not merely block NMDA-R transmission at the electroreceptor afferent to ON cell synapse; ELL granular interneurons also express NMDA receptors (Harvey-Girard et al., 2007) and so this treatment will likely reduce disynaptic GABA-A inhibition as well as block NMDA-R transmission onto ON cells (Fig. 1). Under these conditions, we observed minimal temporal summation (Fig. 2B, left), and short ISIs often resulted in prominent depression of the evoked EPSP (Fig. 2B, right). This is not surprising since there is no longer the slow NMDA-R component capable of temporal summation, thus unmasking the previously characterized depressing AMPA-R component.

We next blocked GABA-A receptors with intracellular PTX but left NMDA-R mediated transmission intact (Fig. 2C, left). Again, we observed strong temporal summation of EPSPs to a plateau potential and the EPSPs evoked after shorter ISIs were smaller; now, however, longer ISIs could also produce this effect (Fig. 2C, right). It

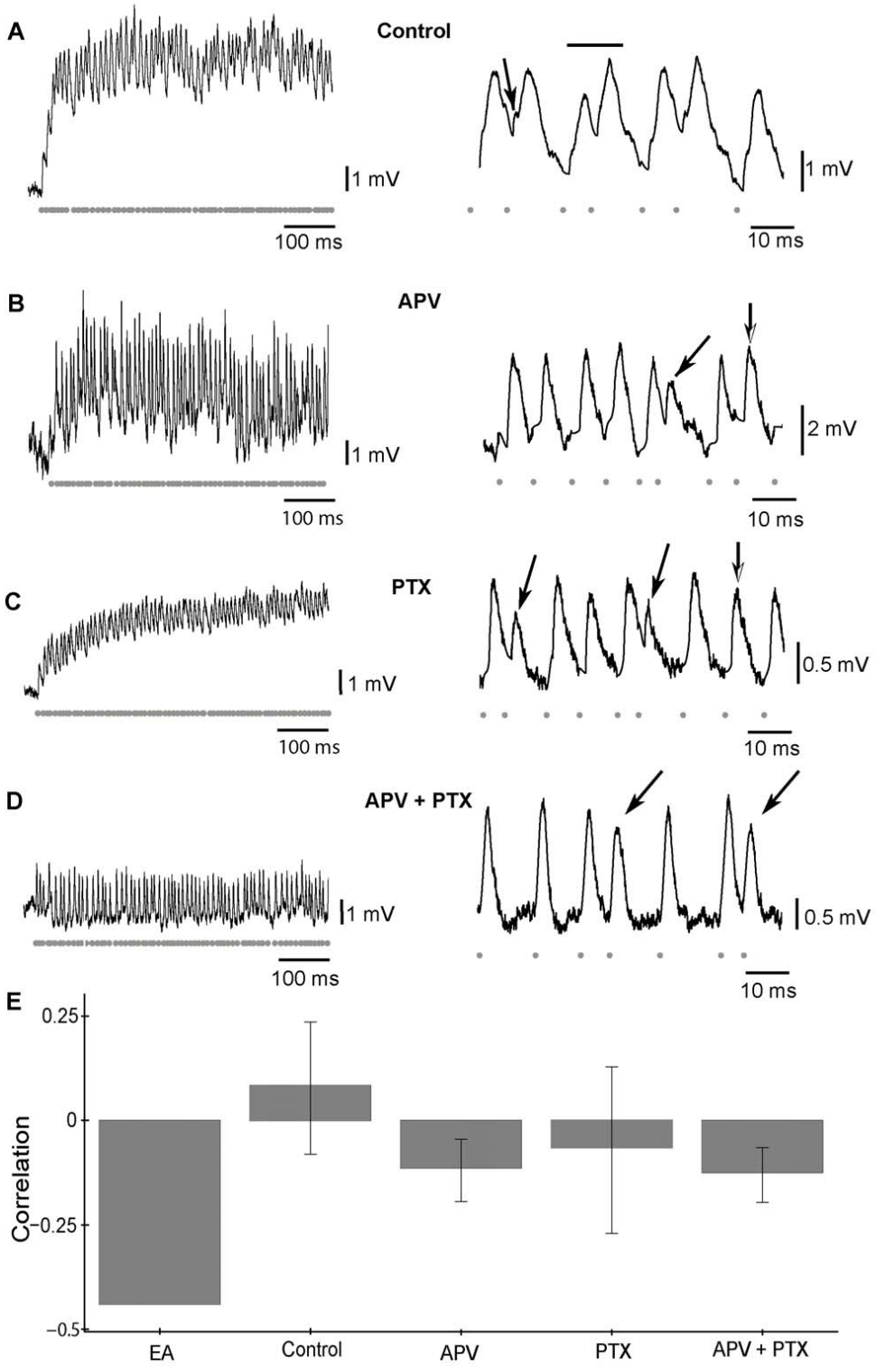
A
Control
1 mV
100 ms
1 mV
10 ms
B
APV
1 mV
100 ms
2 mV
10 ms
C
PTX
1 mV
100 ms
0.5 mV
10 ms
D
APV + PTX
1 mV
100 ms
0.5 mV
10 ms
E
0.25
0
−0.25
−0.5
Correlation
EA
Control
APV
PTX
APV + PTX

Figure 2. Basilar pyramidal cell response to EA fiber stimulation with a natural baseline discharge pattern (gray dots in this and subsequent figures). Intrinsic conductances are removed by intracellular blockade. *A:* Characteristic response to stimulation with AMPA, NMDA and GABA-A receptors intact. Stimulation results in plateauing temporal summation with stimulation (left). Closer examination of the evoked response reveals a complex sequence of EPSPs and IPSPs (right). Note that the fast AMPA-R component of the EPSP (arrow) can be distinguished from the slower NDMD-R component. Short ISIs evoke EPSPs of equal or increasing (bar) amplitude. *B*: EPSPs in the presence of 2-amino-5- phosphonovaleric acid (APV). Minimal temporal summation is seen with NMDA-R blocked (left). Short ISIs result in depression (first arrow), although this is not always the case (second half-arrow) (right). *C*: blocking GABA-A with picrotoxin while leaving NMDA-R intact results in strong temporal summation to a plateau potential (left). Short ISIs resulted in depressing EPSPs (first two arrows), although longer ISIs occasionally had the same result (half-arrow right). *D*: Blocking both NMDA and GABA-A receptors once again eliminated temporal summation. Short ISIs result in prominent depression (arrows). E: Serial correlations between the heights of successive EPSP peaks evoked by EA stimulation sequence obtained from a natural baseline EA discharge pattern. The EA ISIs had a negative serial correlation coefficient of -0.44. Two-tailed t-tests were performed to determine if the mean serial correlations differed significantly from 0. Blocking intrinsic conductances (control) eliminated the negative serial correlation (0.083, SD = 0.16, N = 10, p = 0.13). Negative correlation re-appeared in the absence of NMDA-R (APV; -0.11, SD = 0.075, N = 6, p = 0.0046) or with both NMDA-R and GABA-A blocked (-0.12, SD = 0.066, N = 5, p = 0.013). Absence of

GABA-A alone did not have a significant effect (PTX; -0.065, SD = 0.19, N = 5, p = 0.50). Both cases in which NMDA-R was blocked (APV, APV+PTX) had mean correlation coefficients that differ significantly from control (one-way ANOVA, p = 0.0188; Tukey post hoc). All conditions had significantly reduced negative amplitude correlations compared to ISI correlations from *in vivo* EAs.

appears that, with inhibition blocked, the NMDA-R component of the EPSPs can summate to a plateau potential and the peaks represent the combined AMPA-R and NMDA-R components.

With both NMDA and GABA-A receptors blocked, temporal summation of successive EPSPs did not occur and no summation to a plateau potential was observed. As seen in Fig. 2D (left), short ISIs result in prominent depression that, as previously shown (Khanbabaie et al., 2010), recovers after only a single longer ISI. Therefore, the temporal summation of EPSPs evoked by short EA ISIs is due to slow NMDA receptor currents, which effectively counteract the fast EA presynaptic short-term depression. Note that the dynamics of disynaptic inhibition (currently unknown) may complicate this effect.

We next computed the serial correlations at lag 1 between successive peak amplitudes of the evoked EPSPs. Two-tailed t test were performed to determine if the mean serial correlations differed significantly from zero. The original EAs had negative ISI serial correlations (-0.44) but in the control case (AMPA, NMDA and GABA receptors intact) these negative ISI correlations were not reflected in any significant correlations between successive EPSP peak amplitudes (Fig. 2E, correlation = 0.083, SD = 0.16, N = 10, p = 0.13, two-tailed t test). Blocking either NMDA (correlation = -0.11, SD = 0.075, N = 6, p = 0.0046, two-tailed t test) or both NMDA and GABA-A receptors (correlation = -0.12, SD = 0.066, N = 5, p = 0.013, two-tailed t test) resulted in the re-appearance of negative serial correlations in the peak amplitudes, while blocking inhibition with PTX application alone did not have a significant effect (correlation = -0.065, SD = 0.19, N = 5, p = 0.5037, two-tailed t test). Indeed, the correlation coefficient

for the control condition differs significantly from both cases in which NMDA is blocked ($p = 0.0188$, one way ANOVA with Tukey post-hoc comparisons) but not when inhibition alone is blocked. For the APV and APV+PTX cases, the small AMPA-R mediated EPSP peaks merely reflect the depression due to a lack of NMDA-R mediated temporal summation (Khanbabaie et al., 2010). On average, the un-masked depression results in higher peaks being followed by smaller ones, and vice-versa, constituting an expression of the negative ISI correlations at the level of synaptic responses. The absence of a significant effect in the case of blockade of inhibition by PTX is presumably due to the residual NMDA-R dependent temporal summation that masks the AMPA-R depression. Note that in all cases, the serial EPSP peak correlation did not reach *in vivo* SC values for the afferent ISIs.

We conclude that, under control conditions, the postsynaptic dynamics of combined direct excitatory plus disynaptic inhibitory electroreceptor afferent input onto E cell dendrites is matched to the EA ISI structure, in the sense that serial correlations between successive EPSP peak amplitudes are eliminated. These uncorrelated peak amplitudes are left to represent the stimulus, consistent with the Nesse et al. (2010) coding scheme, although it does not prove it. The NMDA-R mediated component of the EPSP is most important for this effect because its time course extends over several ISIs and the resulting temporal summation produces a positive correlation that counterbalances the negative correlation imparted by short-term depression of the AMPA-R component.

Signal encoding by pyramidal cells with excitation plus inhibition

An *in vivo* study (Bastian et al., 2004) has shown that the EA input to an ON cell (summed EPSPs/IPSPs) can faithfully reconstruct a low-frequency stimulus presented within its receptive field. Larger functional networks (Chacron et al., 2011) were active in these experiments and might conceivably contribute to the observed stimulus reconstruction. Here, we aimed to determine the synaptic requirements for this reconstruction in the absence of these networks. In order to estimate reconstruction accuracy, we used a spike sequence, recorded from an EA in response to a random amplitude modulation (RAM) stimulus (Fig. 3A, see Methods) to drive the EAs of E cells. We used stimulus-evoked responses from the same EAs that were also used for our analysis of the ON cell response to baseline EA discharge. We then computed the cross-correlation coefficient between the evoked membrane potential and the original RAM stimulus. Again, we blocked voltage-dependent conductances to study the synaptic potentials in isolation in the E cells. Despite the fact that our stimulation protocol induced non-physiological synchronous EA input, the ON cell membrane potential was still able to reconstruct moderate amplitude signals *in vitro* (Fig. 3B), provided both NMDA and GABA-A receptors were not blocked. The membrane potential clearly followed even the small modulations of the original stimulus.

Signal reconstruction is significantly impaired with NMDA-R blocked by APV but with inhibition intact; in particular, the response to the small modulations is now absent, although the response to the large dip in the RAM (trough) is still evident (Fig. 3C). At the maxima of the amplitude modulations, pyramidal cells are receiving increased excitatory input; however, with NMDA receptors blocked, there is no temporal summation and the AMPA-R mediated EPSPs become depressed. This is due to fast

AMPA receptor mediated short-term depression (Khanbabaie et al., 2010) acting in concert with the GABA-A disynaptic inhibition as described above. It is not surprising that temporal summation of EPSPs is required to encode a low-frequency signal and that slow NMDA-R mediated synaptic currents are responsible for this encoding. Therefore, with NMDA-R currents intact, we expected efficient and possibly better than the control signal coding in the absence of GABA-A inhibition.

Surprisingly, upon blocking inhibition with PTX, pyramidal cell encoding of amplitude modulations was almost completely eliminated (Fig. 3D). It appears that, in the absence of inhibition, the NMDA-R mediated EPSPs summate to a saturated plateau potential and can no longer encode the variations in electroreceptor afferent input. When both NMDA- and GABA-A receptors were blocked there was no modulation at all in response to the EA stimulation. AMPA receptors alone are not capable of encoding even strong sensory input (Fig. 3E).

As summarized in Fig. 3F, good stimulus reconstruction was only obtained when both NMDA and GABA-A receptors were intact (RAM-response cross-correlation= 0.53, SD = 0.091, N = 10). The mean cross correlation in the APV (cross-correlation= 0.10, SD = 0.19, N = 5), PTX (cross-correlation= 0.18, SD = 0.10, N=6) and APV+PTX (cross-correlation= -0.14, SD = 0.22, N=5) cases were significantly different from control (one-way ANOVA, $p \leq 0.001$; Tukey post hoc). Two-tailed t test revealed that the control ($p \leq 0.001$) and APV ($p = 0.008$) conditions were significantly different from 0, while PTX ($p = 0.30$, two-tailed t test) and APV+PTX ($p = 0.23$, two-tailed t test) were not. We conclude that the relative proportions of excitation and inhibition in the *in vitro* control case are required to encode electrosensory signals by ON cells. The NMDA-component

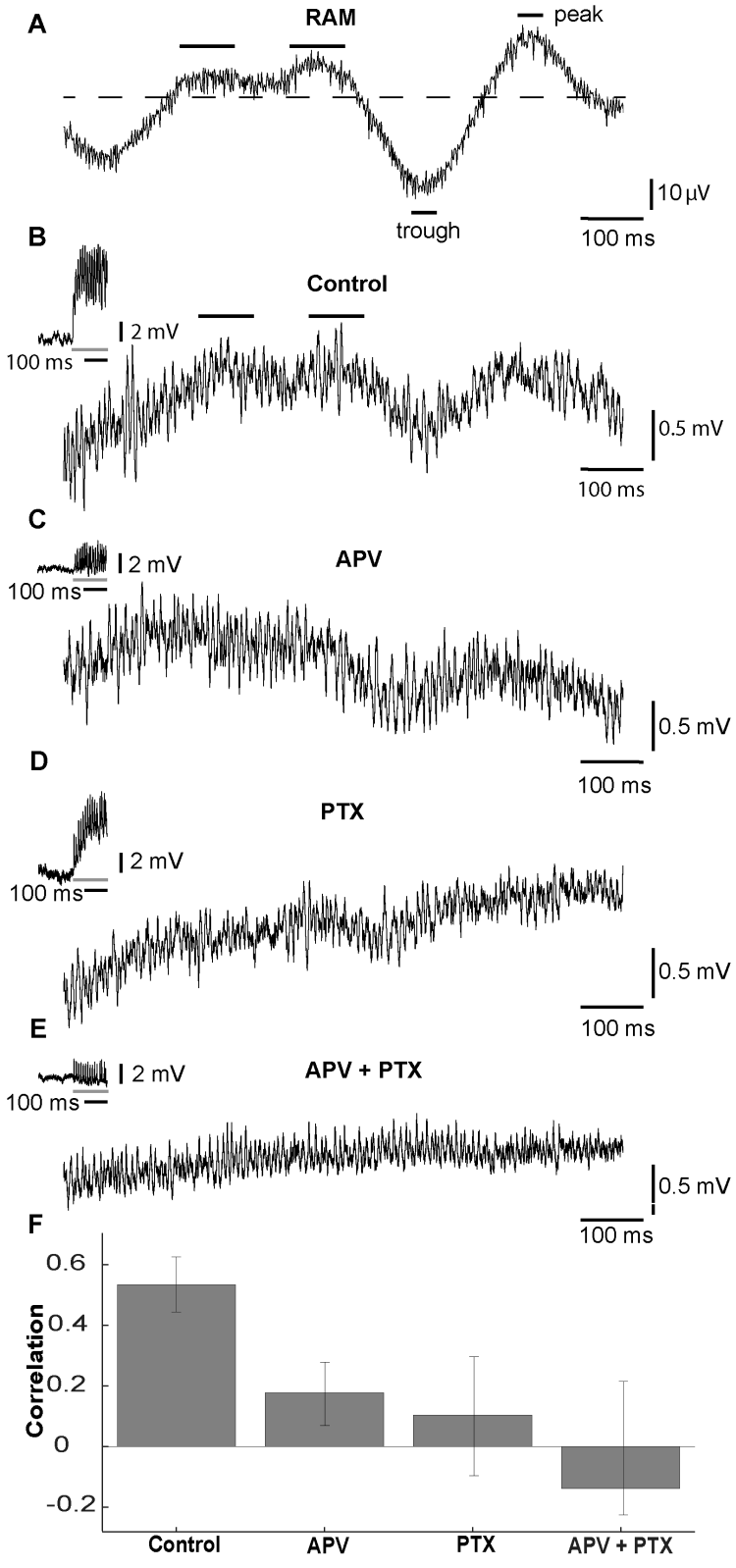
A
RAM
peak
trough
10 µV
100 ms
B
Control
2 mV
100 ms
0.5 mV
100 ms
C
APV
2 mV
100 ms
0.5 mV
100 ms
D
PTX
2 mV
100 ms
0.5 mV
100 ms
E
APV + PTX
2 mV
100 ms
0.5 mV
100 ms
F
Correlation
0.6
0.4
0.2
0
-0.2
Control
APV
PTX
APV + PTX

Figure 3. Stimulus reconstruction from pyramidal cell voltage traces. Pyramidal cell membrane fluctuations were evoked by stimulation of EAs with *in vivo* derived EA spiking responses to RAMs. *A*: RAM stimulus from which electroreceptor afferent spiking responses were obtained**.** Two left bars indicate weak stimulus fluctuations (bumps) mentioned in the text. "Peak" and "trough" bars indicate stimulus regions further analyzed in Figure 5. *B-D:* In each case, 10 pyramidal cell responses to electroreceptor afferent input were averaged. *Insets*: pyramidal cell responses at stimulus onset (gray bar). *B:* Inset: stimulation leads to temporal summation to a plateau potential; main figure is taken from the steady state response. With intrinsic conductance's blocked and AMPA, NMDA and GABA receptors intact, membrane fluctuations can reconstruct even weak amplitude modulations (bars). *C:* Inset: in the presence of APV, no plateau potential is observed. In the absence of NMDA-R (APV), there is no temporal summation (*inset*) and signal reconstruction is impaired. *D:* Inset: in the presence of PTX temporal summation to a plateau potential is observed. With GABA-A receptor mediated inhibition blocked, weak signal reconstruction is eliminated even though both AMPA-R and NMDA-R are intact. This suggests that, in the absence of inhibition, NMDA-R mediated EPSPs summate to a plateau potential and are no longer able to encode changes in the afferent input. *E:* Inset: in the presence of APV and PTX, no plateau potential is observed. AMPA receptors alone are not capable of encoding even strong sensory input. *F*: Mean cross-correlation between evoked pyramidal cell membrane potential fluctuations and the RAM stimulus (+/- SD). The stimulus was well reconstructed with NMDA-R and AMPA-R intact (cross-correlation 0.53 SD = 0.091, N = 10). Cross-correlation was significantly reduced in APV (0.10, SD = 0.19, N = 5), PTX (0.18, SD = 0.10, N=6) and

APV+PTX (-0.14, SD = 0.22, N=5) cases. All conditions have means significantly different from control (one-way ANOVA, $p \leq 0.001$). Two-tailed t-tests revealed that the control ($p \leq 0.001$) and APV ($p = 0.0080$) conditions were significantly different from 0, while PTX ($p = 0.3038$) and APV+PTX ($p = 0.2322$) were not.

of the evoked EPSP must summate to permit an encoding of the slow time scale of the input RAM (0-4 Hz). By itself, NMDA summation will result in a saturated response that no longer follows the stimulus fluctuations. Fast disynaptic inhibition (Berman and Maler, 1998; Khanbabaie et al., 2010) is required to prevent saturation and keep the NMDA-R excitation within its dynamic range.

In order to get a deeper appreciation of these effects, we examined the ON cell responses to the regions in Fig. 3, designated as "trough" and "peak," of the low frequency stimulus (Fig. 4). It is noteworthy that, in all treatment conditions, the EPSP peaks evoked at the local stimulus trough are larger than those evoked at the local peak. This is simply due to the fact that the decrease in stimulus intensity during a trough (below the baseline EOD amplitude) causes a reduction in EA discharge (Gussin et al., 2007) and this in turn results in longer than average EA ISIs. These long ISIs do not cause depression at EA synapses (Khanbabaie et al., 2010). In contrast, the shortened ISIs in the EAs during a stimulus peak cause strong depression and therefore reduced EPSP peak amplitudes.

In the control case (Fig. 4A), the EPSPs during a stimulus trough are large with clear AMPA- and NMDA-R mediated EPSPs, cleanly separated by strong hyperpolarizing events that are likely caused by disynaptic GABA-A inhibition. Although the peak EPSPs are large (~5 mV), they occur while the cell is hyperpolarized (Fig. 4A, left) and these EPSPs rarely trigger spikes in response to sensory input that falls below the baseline EOD amplitude (Bastian et al., 2004). During the peak response, much smaller fluctuations of the membrane potential (~1 mV) are observed riding on the slow NMDA-R mediated depolarization (Fig. 4A, right). Similar results are obtained after

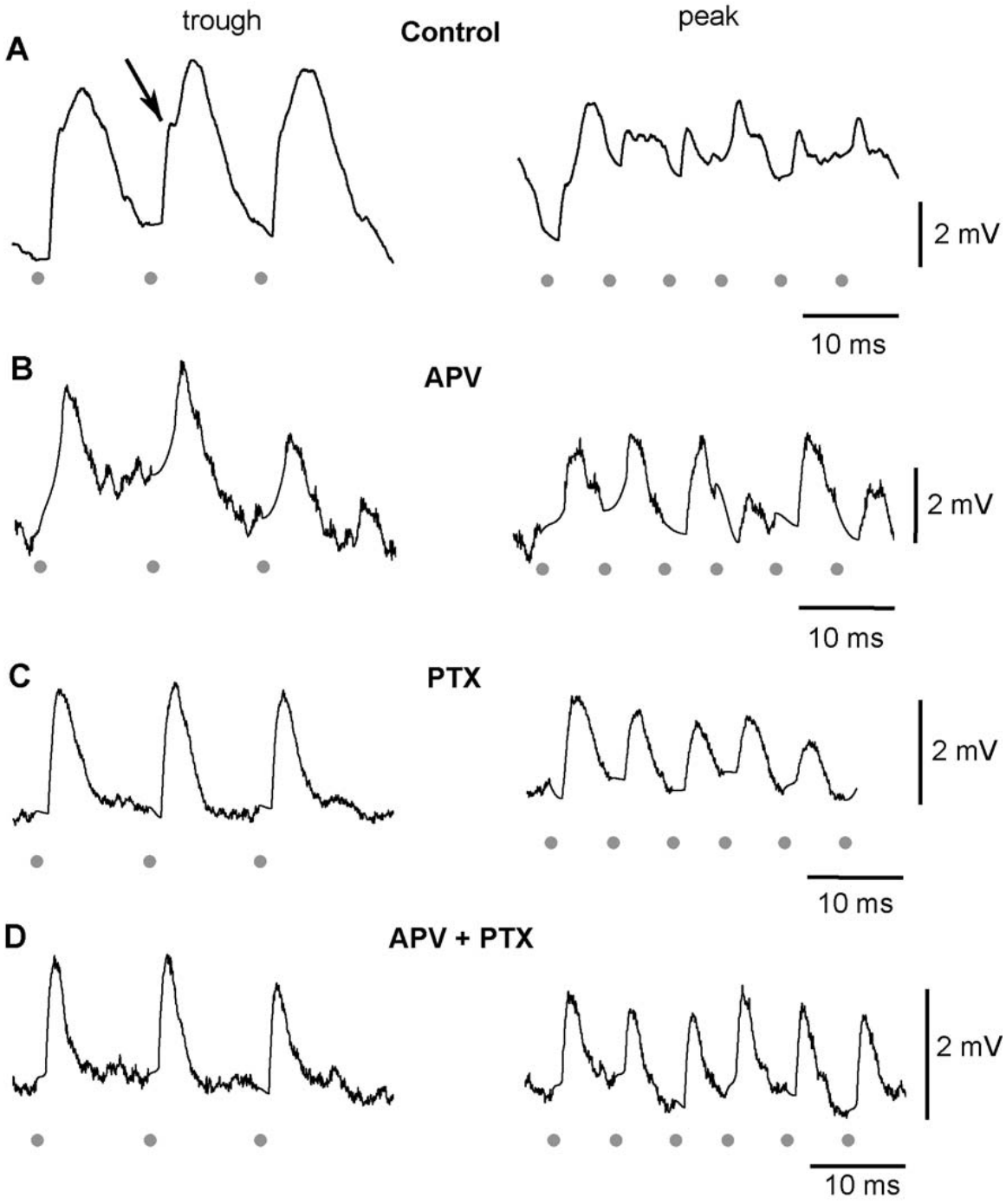
trough
Control
peak
A
2 mV
10 ms
B
APV
2 mV
10 ms
C
PTX
2 mV
10 ms
D
APV + PTX
2 mV
10 ms

Figure 4. Pyramidal cell responses evoked from stimulation of electroreceptor afferents using *in vivo* derived electroreceptor afferent spiking responses to RAMs. The 'peak' and 'trough' were the sections of the response defined by the named bars in Fig.3. Individual EPSPs at the peak (left) and trough (right) of the RAM signal were examined. *A, left:* When intrinsic conductances are blocked, EPSPs have distinct AMPA-R (arrow) and NMDA-R mediated components. *A, right*: At stimulus peak, small membrane potential fluctuations are seen riding on the top of the slow NMDA depolarizations. *B, C, D*: Under all conditions, EPSPs at the stimulus trough are larger in amplitude than those evoked at the stimulus peak.

application of the drugs (Fig. 4B-D), the notable differences being that the EPSPs at the peak are more prominent than for the no drug condition and that blocking inhibition with PTX application (with or without APV) application results in less variability in EPSP amplitude at both the peak and the trough.

Two important issues are raised by these results. First, it is not clear whether the disynaptic GABA-A receptor-mediated inhibition is merely acting as a tonic inhibition that prevents NMDA-R mediated saturation of the responses to the RAM stimulus, or if it plays a more active role in stimulus coding. Secondly, it is not clear to what extent the remaining potential fluctuations in peak response are due to the artificial synchronous stimulation of the EAs. We deal in turn with these issues in the following sections.

Fast disynaptic inhibition can encode slow signals

Since the absence of disynaptic inhibition prevented signal reconstruction (Fig. 3D), we wanted to determine whether GABA-mediated synaptic transmission contributed to the coding of these signals or simply prevented the NMDA-R component of the summating EPSPs from saturating. This was achieved by examining the RAM-stimulus evoked response of OFF cells (see Fig. 1 for OFF cell circuitry), which receive only inhibitory GABA-A input from their receptive field center and are excited by spatially averaged surround input, generated by gap junction input from granular cell dendrites (Maler, 1979; Maler et al., 1981; Berman and Maler, 1998; Bastian et al., 2002). The OFF cells, as expected, inverted the response to the RAM signal (Fig. 5). Remarkably, they were able to accurately follow even the small amplitude modulations (Fig. 5). A stimulus-response cross-correlation value of –0.64 (SD = 0.17, N=5) was attained and, although sign inverted, its absolute value was not significantly different from that

obtained for E cells (p= 0.53). Blocking inhibition with PTX abolished the OFF cell's response to EA stimulation as expected from a previous study (Berman and Maler, 1998; Harvey-Girard and Maler, 2013). The cell's membrane potential simply randomly drifted up and down, and the negative correlation between the OFF cell response and the RAM signal (cross correlation 0.057, N=1) was eliminated, demonstrating that its response did indeed arise from disynaptic GABA-A mediated inhibition. The same GABAergic interneurons send projections to both ON and OFF cells (Maler and Mugnaini, 1994). Since these projections convey information sufficient for stimulus encoding in the OFF cells, we conclude that they also convey the same information to the ON cells. These results demonstrate that the ability of an ON cell's membrane potential to encode RAM signals is likely due to the dynamic balance of NDMA-R mediated excitation and GABA-A mediated disynaptic inhibition.

Computational analyses suggest that asynchronous *in vivo* synaptic potentials are smoother than those evoked by synchronous *in vitro* stimulation and are unlikely to evoke spikes

An unavoidable caveat of our *in vitro* stimulation protocol is the synchronous activation of multiple EAs that would otherwise fire asynchronously *in vivo*. EAs are probabilistic encoders, each firing at a given phase of the EOD waveform but skipping an intermittent number of EOD cycles (Gussin et al., 2007). *In vivo*, populations of EAs that converge onto a pyramidal cell (25 for CMS map) (Maler, 2009a) will fire independently when driven by low frequency stimuli (Benda et al., 2006). Under baseline conditions or when driven by low frequency prey mimic signals, various subsets of the EA population

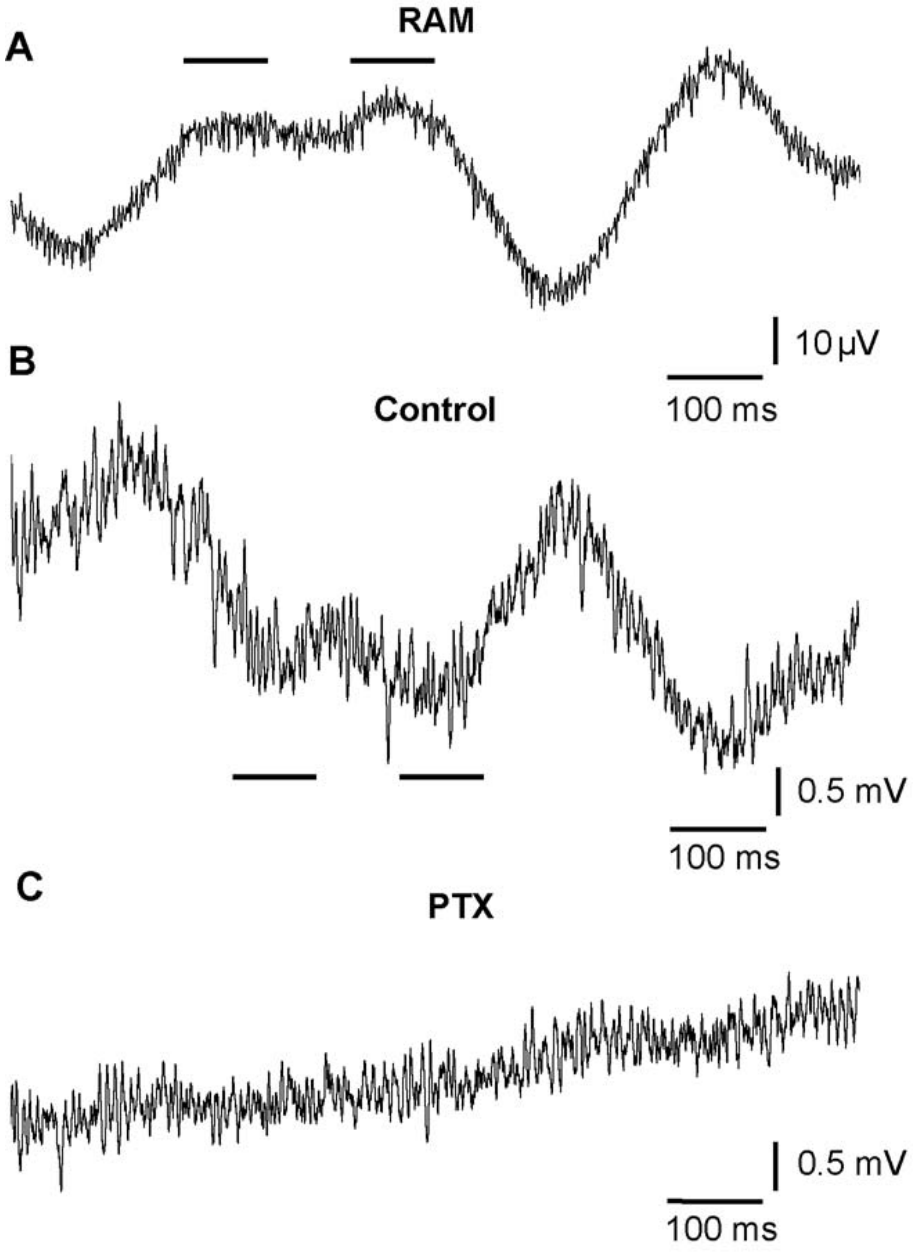
A
RAM
10 µV
100 ms
B
Control
0.5 mV
100 ms
C
PTX
0.5 mV
100 ms

Figure 5. Electroreceptor afferent evoked response of OFF cells to the RAM stimulus. *A*: RAM stimulus from which electroreceptor afferent spiking response was obtained. *B, C:* In each case, 10 pyramidal cell responses to electroreceptor afferent input were averaged. *B:* Membrane fluctuations of OFF cells inverted the RAM signal (cross correlation = –0.64, SD = 0.17, N=5). *C:* Application of PTX completely eliminated the inverse correlation (cross correlation 0.057, N=1), demonstrating that the response arose from GABA-A mediated inhibition.

will discharge in every single cycle of the high frequency EOD, but will not all discharge synchronously. However, for our *in vitro* experiments, the strong pulses used to reliably stimulate the EA fibers in slice are derived from one EA spiking response to a RAM stimulus (Figs. 3, 4 and 5). As a result the stimulated population is entrained to the activity patterns of our exemplar unit (see Methods), firing synchronously within a given EOD cycle and producing an absence of spikes in many others. For example, in Fig. 4 (control, right, peak response) the stimulus pulses skip 2 to 4 EOD cycles. The strong stimulus likely evokes a response in most or all of the 25 EA afferents contacting the ON cell and generates a maximal response. The stimulus used for the *in vivo* recording that generated this EA spike train would result in a peak EA probability of discharge of ~0.33 (Gussin et al., 2007). Therefore, *in vivo*, we would expect that ~8 (one third) of the EA afferents discharged on each EOD cycle and evoked a weaker (one third of maximum *in vitro*) EPSP. Intuitively, one would expect the asynchronous case to generate smoother summed synaptic potential because of the 'filling in' of each EOD cycle with smaller EPSPs and the temporal summation of evoked responses. We lack a detailed understanding of EA-evoked disynaptic inhibition in ELL, and cannot therefore directly model the effect of natural synaptic input on the smoothness of the summed ON cell response. Below, we provide a simple approximate statistical analysis of the heights of the EPSPs that illustrates the magnitude of our hypothesized smoothing effect.

We assume that 25 EAs converge onto the CMS ON cell (Maler, 2009a) and, during the peak stimulus response (Figs. 3, 4), have a mean discharge probability = 0.33. In the artificial *in vitro* case, with stimulation by the one EA exemplar, on each EOD cycle the input is 0 or 25 EAs. This is a discrete density with 0 having a probability of 2/3

and 25 a probability of 1/3. The first moment (i.e. mean) of this density is $\mu_1 = \sum xP(x)$ =0(2/3)+25(1/3)=8.33, the second moment is $\mu_2 = \sum x^2 P(x)$ =(25^2)/3=208.3. The variance of the EPSP height can then be calculated as $\sigma^2 = \mu_2 - \mu_1^2$ = 138.94. In the natural case, on each EOD cycle a fraction of the 25 EAs will independently discharge. This is a binomial density N=25 and p=0.33. The mean will again be Np = 0.33*25 = 8.33 EAs discharging. The variance of the number of EAs that fire in each cycle is Np(1-p)=5.53. The variance of the artificial experimental case is therefore ~25 times greater than the natural case. In order to estimate the evoked response it would be necessary to convolve the EA inputs with a kernel representing the dynamic response of the ON cell to excitatory (AMPA + NMDA receptors) and disynaptic inhibitory input; as mentioned above, this is not possible given our current state of knowledge. Assuming that the variance of the evoked summed EPSP/IPSP response is similar to that of the driving input, we would expect that the standard deviation of the membrane potential at the peak response (Figure 4) would decrease from an estimated 1.8 mV to 0.36 mV. Effectively, the membrane potential would be smooth and without the rapid >2 mV depolarizations that trigger spikes *in vivo* (Bastian et al., 2004; Chacron et al., 2007). In light of this, an obvious question arises: how are pyramidal cell spikes triggered off of this smooth depolarizing response.

Voltage-dependent membrane noise triggers spiking

Previous studies of cortical (Azouz and Gray, 2000, 2003) and ELL pyramidal cells (Chacron et al., 2007) have shown that spiking is evoked by rapid depolarization of the membrane potential, i.e. by steep increases that can be localized in time using the first or second temporal derivative. It is often assumed that AMPA-R mediated currents

provide the necessary rapid depolarization to elicit spiking. In an ELL slice, the rising phase of a single EA evoked EPSP (mostly AMPA-R) will evoke a spike (Berman and Maler, 1998; Khanbabaie et al., 2010). Electroreceptor afferents normally discharge continuously at a high rate (Gussin et al., 2007) and under these conditions the AMPA-R mediated component of the EPSP is slightly depressed (Khanbabaie et al., 2010). We therefore hypothesize that, *in vivo*, it is the NMDA-R and not AMPA-R component of the stimulus evoked EPSP that evokes most spiking in ON cells. Further, our experimental results and statistical analysis suggest that the response to slow increases in EOD amplitude are smooth and lack the rapid depolarizing events (i.e. no large second derivative) required to evoke spikes (Chacron et al., 2007). This prompted us to consider how the slow NMDA-R EPSPs could possibly drive spiking.

Early work in the ELL described the presence of membrane noise that increased in amplitude with depolarization (Mathieson and Maler, 1988); this noise was attributed to voltage-gated ion channels likely selective for Na^+, although a contribution by synaptic noise could not be excluded. Since these rapid membrane potential fluctuations were able to elicit spikes in pyramidal cells *in vitro* (Mathieson and Maler, 1988), we decided to investigate *whether noise could compensate for the depressed AMPA-R component of the EA evoked EPSP and drive the fast upstrokes* in membrane potential required for spiking in pyramidal cells.

We treated the ELL with CNQX and APV to block synaptic transmission onto ON cells and interneurons and therefore eliminated synaptic input as the source of rapid fluctuations in membrane potential. We then recorded from CMS pyramidal cells without any channel blockers (i.e. no QX-314 or cesium in the pipette) and applied depolarizing

current steps; because synaptic transmission was blocked, we were not able to determine whether we were recording from ON or OFF cells. As previously described (Mathieson and Maler, 1988), the pyramidal cell membrane potential was noisy and the amplitude of the membrane potential fluctuations increased dramatically with depolarization (N=5, Fig. 6A). Spike threshold varied across cells but was typically near -65mV. As the membrane potential approached spike threshold, the presence of rapid, large depolarizations (blips) became apparent and *these blips were seen to co-occur with spiking* (Fig. 6B). To investigate the membrane noise in more detail, we computed histograms of the membrane potential at different levels of depolarization. The membrane noise histograms were well fit by the Gaussian distribution at relatively hyperpolarized levels (Fig. 7A). However, at more depolarized levels (near threshold) the distribution has a higher variance (Fig. 7B, C) and becomes both more peaked (kurtotic) and positively skewed to the right (Fig. 7B, D). The positive skew is due to an increase in the occurrence of the large blips. When we included voltage-gated ion channel blockers in the pipette, the variance was low and independent of membrane potential (Fig. 7C inset, N=1) conclusively identifying the noise as intrinsic rather than a result of synaptic conductances.

We hypothesize that many stimulus-evoked spikes in ON cells are elicited by the voltage-dependent blips, which would ride on top of the summating NMDA-R component of the PSPs evoked by the EAs. To investigate this possibility, we turned to the centrolateral segment (CLS) of the ELL and repeated the noise experiments described above (N = 5). We switched to the CLS map because preliminary experiments had shown

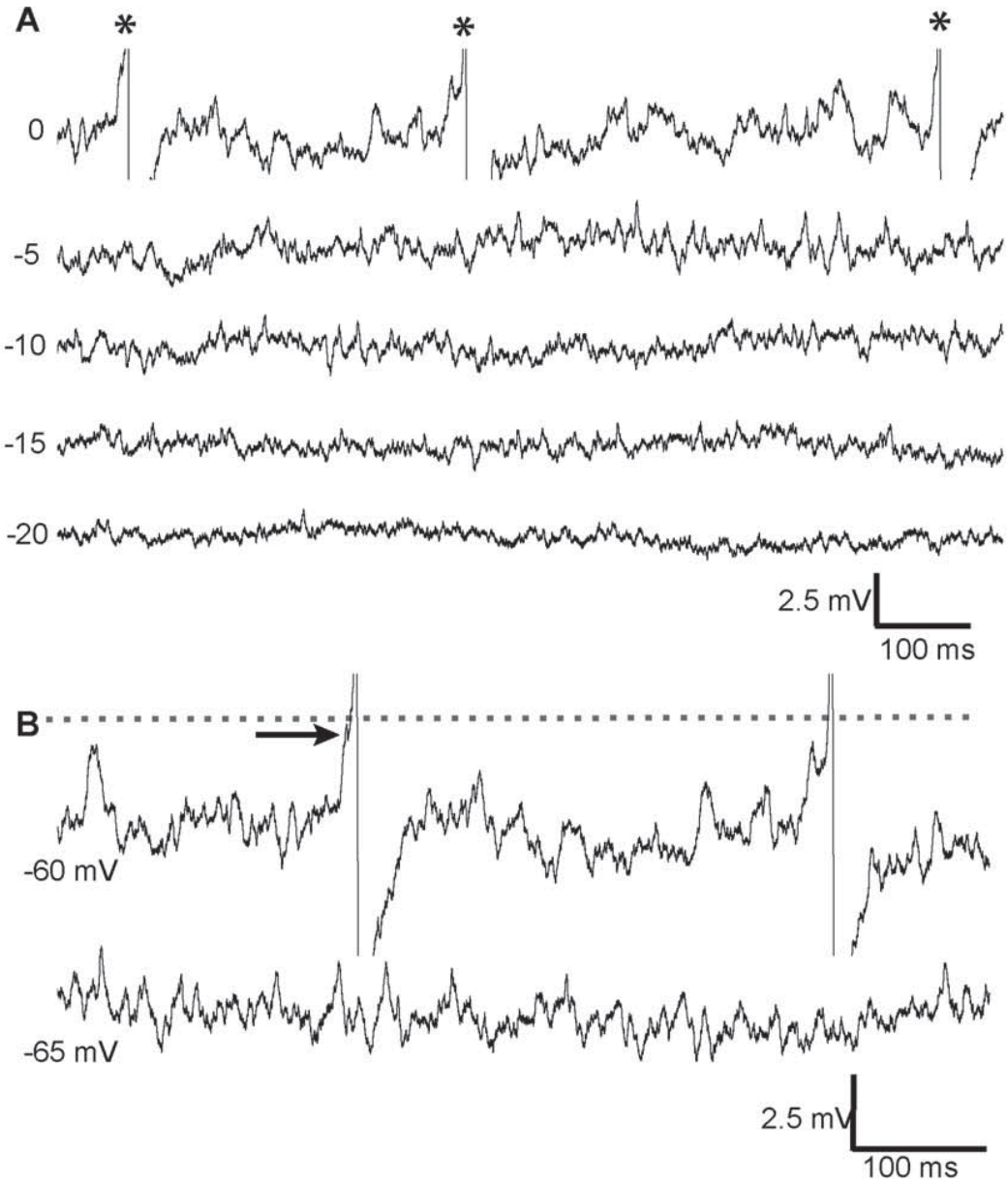
A
*
*
*
0
-5
-10
-15
-20
2.5 mV
100 ms
B
-60 mV
-65 mV
2.5 mV
100 ms

Figure 6. Recordings of spontaneous pyramidal cell membrane potential at various holding potentials. Recordings were taken with extracellular CNQX and APV to block synaptic noise. *A*: Amplitude of membrane potential fluctuations increases dramatically with depolarization to spike threshold (around -65 mV, here normalized to 0). Near threshold, rapid large depolarization elicits spiking (*, spikes truncated). *B*: Blips elicit spikes (arrow) when they reach spike threshold (dashed line). Here we give the absolute membrane potentials for this particular neuron – the traces (top: -60 mV; bottom: -65 mV) are an expanded version of the normalized top traces of A (0, -5).

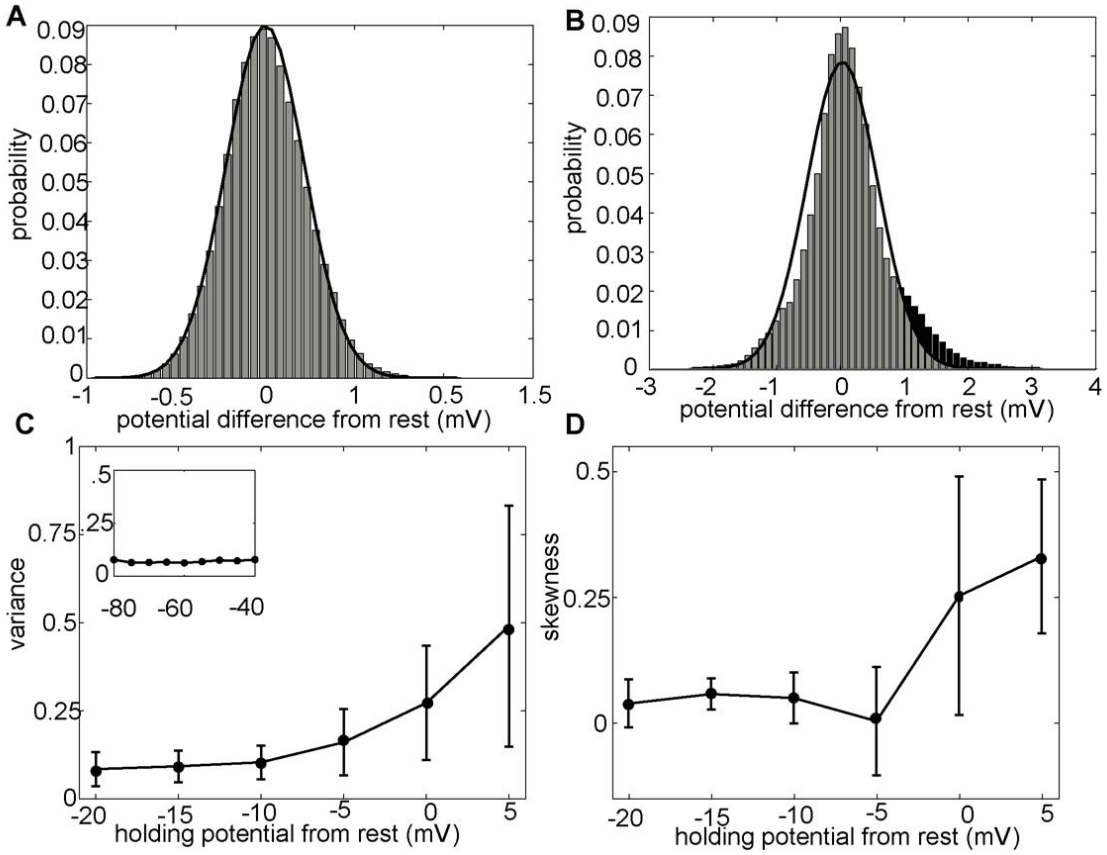
A
probability
potential difference from rest (mV)
B
probability
potential difference from rest (mV)
C
variance
holding potential from rest (mV)
D
skewness
holding potential from rest (mV)

Figure 7. Probability distribution, variance and skew of CMS pyramidal cell membrane fluctuations. Recordings were made with extracellular CNQX and APV to block synaptic noise. The resting membrane potential was simply the neuron's mean potential without any current injection. In the following panels, we normalized each recording by subtracting this mean potential so as to display more clearly the effect of injecting de- or hyper-polarizing current. *A*: When hyperpolarized, pyramidal cells membrane noise histogram (gray) is well fit by a Gaussian distribution (black curve overlay). *B*: Near threshold, the distribution is more peaked (kurtotic) and positively skewed than the best fit Gaussian distribution. The skew in the distribution (black) is likely a result of an increased frequency of rapid depolarizations (blips). *C, D:* Holding potentials are normalized to spike threshold, with 0 representing spike threshold. *C*: Variance of noise distribution increases with depolarization. *Inset*: When voltage gated ion channels were blocked, variance was reduced and became independent of membrane potential, demonstrating an intrinsic source of noise. *D*: Skew increases dramatically at potentials at or above spike-threshold.

that the blip events (right tail of the distribution shown in Fig. 7B for the CMS map) were far more prominent, allowing us to determine blip occurrence with greater fidelity and temporal accuracy. The overall membrane noise characteristics were otherwise identical to the CMS map: CLS pyramidal cells display fluctuations whose variance and skewness increase with depolarization of the membrane potential (data not shown).

Figure 8A shows an example membrane potential trace from a CLS neuron, demonstrating clear blips and the occasional spike. The figure inset shows that an action potential may trigger directly off the peak of a blip (indicated by the dashed arrow). Furthermore, the blip waveform has an onset slope nearly identical to the AMPA-R component of an EPSP (shown in gray, overlaying the excised blip), suggesting that these noisy fluctuations are sufficient to trigger spikes when they occur near the action potential threshold. Using the same derivative criteria as was used above to identify spikes, we isolated the times at which blips occurred and computed inter-blip interval statistics including the serial correlation coefficients of inter-blip intervals (IBpI) and the IBpI histogram. The IBpIs had means ranging between 0.39 s (SD =0.23) and 0.22 s (SD = 0.25) for the 3 CLS cells where blips could be cleanly extracted. The IBpI showed no serial correlation (Fig. 8Bi, black circles) indicating that the blips originate from a renewal process. We found the IbpI distributions were consistent with the renewal process being either a Poisson (Fig. 8C; left, top) or a more general gamma process (Fig. 8C; left, bottom), depending on the neuron.

To determine whether the statistical patterns of blip generation might influence the statistical patterns of pyramidal cell spiking, *in vivo* extracellular recordings were obtained from CLS pyramidal neurons in the absence of a stimulus (N ON cells = 5, N

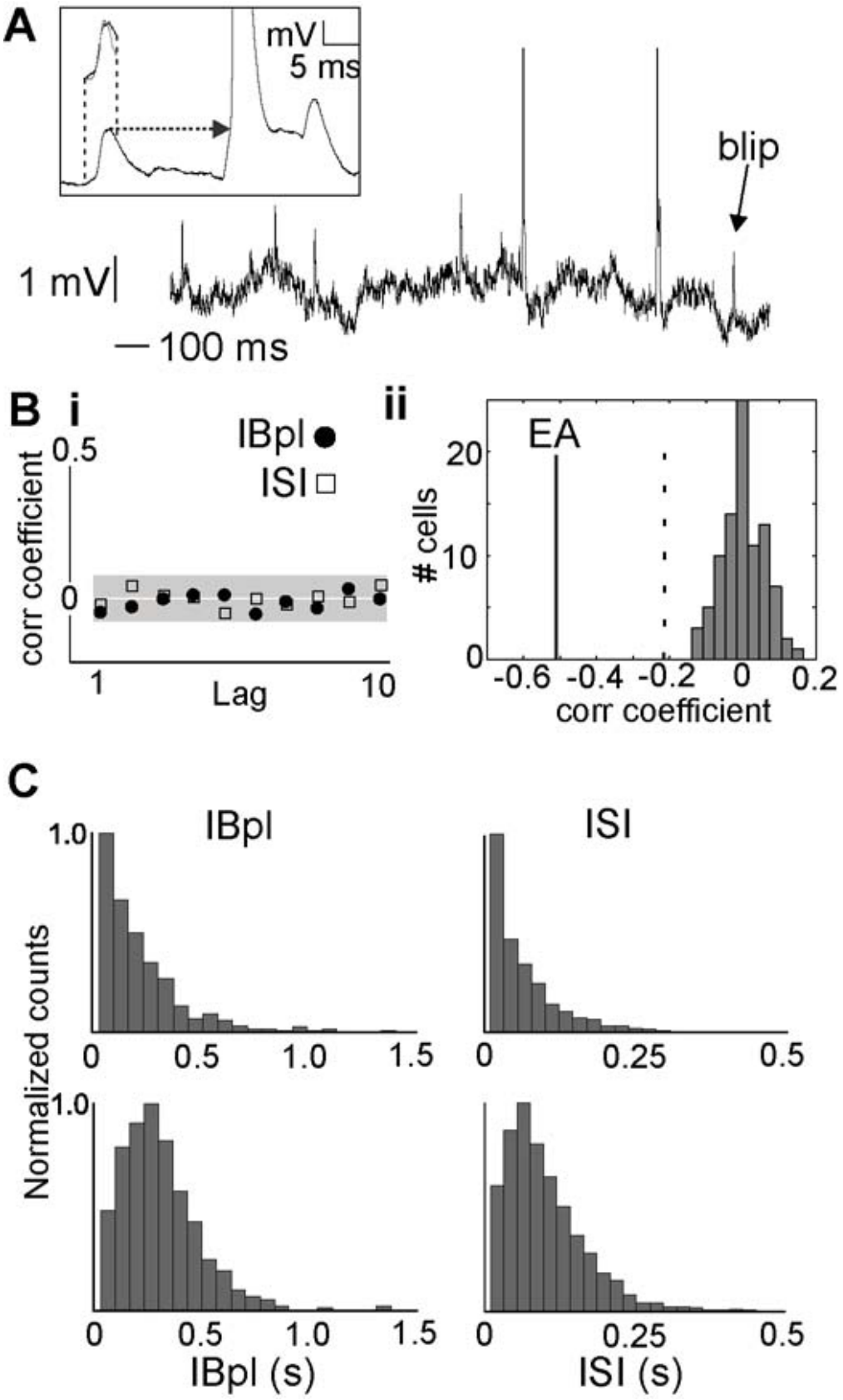
A
mV
5 ms
blip
1 mV
100 ms
B i
IBpI
ISI
corr coefficient
0.5
0
1
Lag
10
ii
EA
cells
20
10
0
-0.6 -0.4 -0.2 0 0.2
corr coefficient
C
IBpI
ISI
Normalized counts
1.0
0 0.5 1.0 1.5
0 0.25 0.5
IBpI (s)
ISI (s)

Figure 8. Statistical structure of blips and of pyramidal cell spiking to which they contribute. *A*: An example membrane potential trace from the spontaneous activity of an E type pyramidal cell of the CLS map, showing many clear blips and two action potentials (truncated). The inset shows that the peak of a blip (start of arrow) is at the same height as the inflection point (arrow) for an action potential, suggesting that blips may trigger spikes. The thin dashed vertical lines enclose the blip waveform (gray) with a superimposed waveform of the AMPA-R component of an EA evoked EPSP (black). The onsets of the two waveforms are nearly identical suggesting these blips might trigger spikes as effectively as the rising phase (AMPA-R) of EA evoked EPSP. *Bi*: The inter-blip intervals (IBpI, black circles) are not serially correlated and are therefore a renewal point process (left); this lack of correlation is also seen in the ISI sequence derived from the spiking output of the ELL pyramidal cells (ISI, open squares). *Bii*: A histogram of serial ISI correlations from a larger (N=91) sample of CLS ON and OFF cells (firing rates between 5 and 35 spikes/s). Correlations are mostly within ±0.1 with an average near 0. We also illustrate the strong mean negative serial correlations of EAs (black line, -0.52) and the highest correlation observed (dashed line, -0.23); note that there is no overlap between EA and ON/OFF cell correlations. *C*: We found two patterns of IBpIs (left), which are both reflected in the ISI statistics of individual ELL pyramidal cell neurons from the centrolateral map (right). This strongly suggests that blips directly drive a portion of spikes in ELL pyramidal cells.

OFF cells = 5). Examination of the data showed that there were no significant differences between ON and OFF cells and the data was therefore pooled. The mean ISIs of the 10 cells ranged between 0.13 s (SD= 0.13) and 0.039 s (SD= 0.025). The mean ISIs are significantly smaller than the mean IBpIs, presumably due to the cells being driven more strongly by the EAs and feedback *in vivo,* rather than by intracellular current injection *in vitro*. As illustrated in Fig. 8Bi (open squares), this small sample suggests many *in vivo* ISIs are not significantly correlated at any lag demonstrating that some ON and OFF cell spiking follows a renewal process. Because there are some apparently contradictory results in the literature concerning ELL pyramidal cell serial ISI correlations (see Discussion), we also examined the distribution of baseline ISI serial correlations in a much larger sample of previously recorded CLS ON and OFF cells (Clarke et al., 2014). We had a sample of 50 ON cells (firing rates of 6.3 - 35.4 spikes/s) and 41 OFF cells (firing rates of 5 - 30.7 spikes/s). Preliminary analysis showed that there serial ISI correlations were not significantly different in the two populations and so the data were pooled for a sample of N= 91 cells. As illustrated in Fig.8Bii, the ISI correlations are all low (mean 0.003; ±0.059), and include both small positive as well as negative correlations ranging between -0.1 and +0.1. In contrast, we also illustrate the EA serial ISI correlations taken from Ratnam and Nelson (2000). These have a mean of -0.52 ±0.14 (black line under EA) and a range of -0.23 to -0.82. The lower value (-0.82) is off the scale of the figure, and a dashed line indicates the maximum correlation (-0.23) observed. It is clear that, in going from EAs to pyramidal cells, there is a massive reduction in ISI correlations, and that the ON and OFF cell serial correlations are, for the cells with firing rates <40 spikes/s, near zero.

The *in vivo* ISI histograms qualitatively match the two classes of IBpI histograms observed in our *in vitro* experiments (Fig. 8C, left vs right). We hypothesize that the blip voltage-dependence generates an optimal noise level for the encoding and transmission of sub- and peri-threshold low-frequency signals by ON cells, i.e. blips are the basis for ON cell stochastic resonance. Further, we hypothesize that blips form a basis for a renewal point process, which is conserved in the spiking output of the ELL pyramidal cells, even *in vivo* when the ON or OFF cell functions as part of the entire network. Together with the decorrelation of EPSP peaks by the natural mixture of synaptic currents, the renewal blip-process ensures an efficient encoding of stimulus amplitude modulations centrally, including for signals that lie below or in the vicinity of the spiking threshold.

Discussion

Our *in vitro* study reveals how excitatory and inhibitory synaptic transmission to ON pyramidal cells and their intrinsic noise combine to encode electrosensory signals transmitted by the EAs.

A) Elimination of EA ISI correlations.

The EA ISI correlations are not transmitted to serial correlations of EPSPs peaks because of the NMDA-R component of the EPSPs; the AMPA-R component, on its own, will transmit the correlation (Fig. 2E). This is expected because the AMPA-R EPSP component shows a rapidly recovering depression after short ISIs (Khanbabaie et al., 2010). Therefore a short ISI will evoke a depressed second AMPA-R EPSP; the following longer ISI (due to the negative ISI correlation at lag 1) will evoke a larger AMPA-R EPSP. A sequence of a long ISI followed by a short ISI will, by the same

reasoning, evoke a large followed by a small AMPA-R EPSP. In this manner, AMPA-R transmission will, on its own, preserve the ISI negative serial correlations in the EA as negative correlations of the EPSP peak amplitude (AMPA-R component).

The EA synapses onto ON cells utilize NMDA-Rs (Berman et al., 2001; Harvey-Girard et al., 2007) with long evoked EPSPs (Berman and Maler, 1998) (>100 ms), greatly exceeding the mean baseline EA ISIs (~5 ms) (Gussin et al., 2007). The NMDA-R evoked EPSP time scale is better matched to the low firing rates (mostly < 20 Hz or > 50 ms and ~10 EA ISIs) of our sample of ON/OFF cells; again the long ON cell ISIs would be expected to reduce or eliminate the effect of EA ISI correlations. We hypothesize that temporal summation of EPSPs over many ISIs due to NMDA-R effectively eliminates EA negative ISI correlations.

An earlier study (Chacron et al., 2007) showed, in a small sample, that ON and OFF cells with a low firing rate (<20 Hz) showed minimal serial ISI correlations, consistent with our observations on a much larger sample (Fig. 8Bii). These authors did show that pyramidal cells with a higher firing rate (>40 Hz; in our sample all rates were < 40 Hz) did show negative serial ISI correlations (-0.1 to -0.3). Chacron et al. (2007) attributed to an intrinsic mechanism (threshold fatigue) and not to the EA input and this result is therefore also consistent with our analyses. We hypothesize that the negatively correlated fluctuations in AMPA-R potential amplitudes constitute high-frequency synaptic noise that might potentially corrupt the low firing rate ON cell response to low-frequency prey signals. The NMDA-R component therefore eliminates this noise source and also matches the ON cell response to the low-frequency input associated with e.g., prey signals.

Theoretical analyses (Nesse et al., 2010) predict that the negatively correlated EA ISIs are caused by quasi-independent peaks of the adaptation variable intrinsic to an EA. Further, the quasi-independence of the adaptation variable could be recovered postsynaptically provided that the synaptic kinetics were matched to those of the EA adaptation process. This representation in terms of independent variables could, in theory, implement an efficient encoding strategy. The elimination of postsynaptic negative serial correlations is a signature of such matching and is thus at least consistent with the Nesse et al. (2010) theory. A similar effect has been observed at the single neuron level in cortex although it is implemented by an entirely different biophysical mechanism (Pozzorini et al., 2013). Their analysis strongly suggested that power law spike frequency adaptation performs temporal whitening of inputs. We have provided a direct example of temporal decorrelation (whitening) at the synaptic level, here implemented by the combined activity of NMDA and AMPA receptor currents.

B) Electrosensory signal encoding.

Behavioral experiments have shown that *A. leptorhynchus* can detect weak prey signals (<1 μ V) (Knudsen, 1974; Nelson and Maciver, 1999). Our results suggest that the dynamic balance between NMDA-R-mediated temporal summation and GABA-A mediated inhibition is needed to encode these signals. Blockade of NMDA-R activity eliminates this coding. The importance of NMDA-R transmission is made clear by examining EA synaptic responses during the peaks of the RAMs. The short ISIs induce presynaptic depression of the EPSP AMPA-R component (Khanbabaie et al., 2010) making it unlikely that they will trigger many spikes *in vivo*. We hypothesize that the AMPA-R component merely permits activation of the NMDA-R, but does not contribute

to signal encoding in our CMS ON cell population.

The NMDA-R component of the EPSP does not depress. This is likely due to two factors: temporal summation of these long EPSPs may mask depression and the relative affinity (half-maximal effective concentration, EC50) of glutamate for the AMPA-R (EC_{50}: 500 uM) versus NMDA-R (EC_{50}: <2 uM) (Dingledine et al., 1999). EA afferents are glutamatergic (Wang and Maler, 1994). Glutamate concentrations at the synaptic cleft reach ~1 mM (Clements et al., 1992) with extrasynaptic concentrations reaching 190 uM (Dzubay and Jahr, 1999). We hypothesize that the EA presynaptic depression is due to a reduction of the cleft glutamate concentration below that required for AMPA-R activation, but still adequate to activate NMDA-Rs. The longer time course and positive voltage dependence of the summating NMDA-R EPSP can then effectively encode and amplify low frequency signals extending over many EA ISIs.

The sensitivity to prey signals inferred from our study is likely higher *in vivo*. Our *in vitro* stimulation, based on the response of a few EAs, resulted in the synchronous activation of pyramidal cells. *In vivo* encoding in ELL would arise via asynchronous responses of heterogenous EAs, and better follow small stimulus fluctuations. For practical reasons (see Methods), our synaptic analysis was confined to the CMS. ON-type pyramidal cells in the CMS receive about 25 EA inputs while those in the CLS receive about 100 inputs (Maler, 2009a). CLS ON cells are thus more sensitive to prey mimics in their receptive fields (Chacron et al., 2011; Marsat et al., 2012; Krahe and Maler, 2014) although both maps respond equally sensitively to moving prey mimics (Khosravi-Hashemi and Chacron, 2014).

C) Role of GABA-A mediated inhibition in signal detection.

Blockade of GABA-A transmission alone prevents both ON- and OFF- cells from encoding signals. This might be due to prevention of NMDA-R EPSPs saturation. Saturation does not, however, account for the excellent OFF cells responses to stimuli in their receptive field center relayed by disynaptic GABA-A synaptic input (Maler et al., 1981; Maler and Mugnaini, 1994; Berman and Maler, 1998). Because OFF cell circuitry is complex (Maler et al., 1981; Maler and Mugnaini, 1994) we offer no further speculation on the mechanism(s) by which OFF effectively encode signals (Fig. 1). We simply conclude that ON cell encoding of prey signals requires a balance of direct EA input and disynaptic inhibitory input. Detailed computational analyses will be required to understand the underlying dynamics.

D) Somatic amplification of signal input via voltage-dependent stochastic resonance.

The ON cell response to stimulus evoked EA spike patterns was typically small (<2 mV) and comparable to the responses seen *in vivo* (Bastian et al., 2004). These small depolarizations are not expected to reach spike threshold from the typical *in vitro* resting membrane potential (Mehaffey et al., 2008). Yet, *in vivo*, these small compound EPSPs do evoke a strong spiking response (Bastian et al., 2004) suggesting that some amplification intervenes between synaptic response and spike output. We have shown that somatic persistent sodium channels amplify EPSPs arising in distal apical dendrites (Berman et al., 2001) and hypothesize that the same mechanism will amplify EA input to the ON cell basal dendrites.

We have discovered voltage-dependent membrane noise that is steeply activated

near spike threshold (Mehaffey et al., 2008). The fluctuations have a sharply rising slope resembling that of AMPA-R EPSPs and trigger spiking. Although the precise nature of the underlying stochastic biophysical dynamics is not known for ELL pyramidal neurons, similar voltage-dependent noise has been noted in other systems (Jacobson et al., 2005). Our initial studies suggested that the ELL pyramidal cell noise was due to Na^+ channels (Mathieson and Maler, 1988), while a recent theoretical analysis has suggested that the stochastic closure of K^+ channels is the main contributor to membrane noise (O'Donnell and van Rossum, 2014). We have shown (Fig. 1) that both Na^+ and K^+ (Kv3) channels are distributed over the soma and proximal dendrites of ON and OFF cells (Fig. 1) (Turner et al., 1994; Deng et al., 2005) and that both fast and persistent Na^+ channels are present on the soma and on proximal apical dendrites (Turner et al., 1994; Berman et al., 2001). The biophysical substrates for membrane noise are therefore available in ELL pyramidal cells. The origin of the blips is more difficult to determine. Turner et al. showed that the Na^+ channels on the somatic and dendritic membranes of ELL pyramidal cells were clustered in small "hot spots" (Turner et al., 1994). An untested but interesting idea is that blips might in part be generated by the cooperative interactions of tightly co-localized Na^+ channels.

Whatever the source of the ON cell membrane noise, we hypothesize that it implements a voltage-dependent stochastic resonance effect (SR_{VD}). Through this effect, noise due to blips would provide the crucial amplification step that transforms subthreshold/peri-threshold, input-evoked smooth synaptic responses into ON cell spiking output that correlates with the input. The higher parts of the input signal elicit more noise via the voltage dependence, allowing them to become encoded into spikes

albeit with some stochasticity. In the absence of a sensory input, this voltage-dependent noise underlies the stochastic firing of the ON cell, and as is usual for SR, noise would likely not benefit the encoding of large signals. It is not possible, at present, to experimentally confirm that ON cells use SR to encode low frequency signals. The key test, using intracellular QX-314 application to block noise, would also block spiking. There is, however, supporting evidence for our conjecture. We previously demonstrated that the ON cell membrane potential accurately followed a 4 Hz stimulus within its receptive field center (Bastian et al., 2004). Figure 4 of this paper shows that fast depolarizations ride on top of the slow 4 Hz modulation and drive spiking. We suspect, but cannot prove, that these fast fluctuations seen *in vivo* are due to the membrane noise that we analyzed *in vitro*; although clearly not conclusive, this data is at least consistent with our voltage-dependent SR theory.

There are three consequences of our hypothesis that SR_{VD} drives spiking to weak low frequency signals. First, since spiking is driven by intrinsic noise rather than the rising phase of EPSPs, it should not be phase locked to the EOD. This is indeed observed for all CMS and CLS ON neurons (Krahe et al., 2008) and strongly supports our hypothesis. We note that this is not simply due to all ELL target cells being unable to follow the high frequency discharge of EAs but, rather, a design feature of these ON cells. This conclusion is based on two exemplars. First, one class of ELL interneuron (ovoid cell) is very strongly phase locked to the EOD (Bastian et al., 1993). This is likely due to this cell type having little (Harvey-Girard et al., 2007) or no (Bottai et al., 1997) NMDA-R expression and therefore being driven by EA-evoked AMPA-R EPSPs. Second, a large subset of LS ON cells (precise identity unknown) is also phase locked to

the EOD (Krahe et al., 2008); neither the mechanism nor the consequences for sensory coding are known in this case. Based on analogy with the ovoid cell we predict that, in this cell class, a) EA evoked AMPA-R EPSPs will drive spiking, b) that these cells will have minimal membrane noise and c) they will be most responsive to high frequency AMs.

The second consequence is that, as shown above, pyramidal cell discharge will have renewal statistics in the absence of sensory input, with the same distribution as that of the IBpIs (gamma). Their baseline spike trains are now an ideal basis for inhomogeneous rate coding.

The third consequence is that the spiking response of ON cells receiving overlapping EA input should not display correlations due to common input, i.e. noise correlations. This exact result has been reported by Krahe et al. (2002) for CMS cells driven by random amplitude modulations (RAMs) of the EOD with a cutoff frequency of <20 Hz, providing strong support for our hypothesis. A different study (Litwin-Kumar et al., 2012), recording from the CLS and LS and delivering electrosensory input (RAM, 120 Hz cutoff) to neighboring pyramidal cells' receptive fields, did find noise correlations. The correlations peaked at time delays near 100 ms consistent with common EA input driving spiking via slow (i.e. NMDA-R driven) excitatory input and noise, and not consistent with spiking driven directly by fast synaptic events (i.e. AMPA-R). Again, this result is supportive of our hypothesis. A separate study (Chacron and Bastian, 2008), recording from the CLS and LS neurons (RAM, 120 Hz cutoff), reached partially contradictory conclusions. Correlations were observed upon stimulation within the neighboring ON cells' overlapping receptive field, but these were mostly signal (not

noise) correlations. This result is consistent with that of Krahe et al. (2002) and Litwin-Kumar et al. (2012) and supportive of our hypothesis. Chacron and Bastian (2008) also reported that there were correlations of baseline spiking activity of neighboring ON (and OFF) cells over short time windows. This result is apparently not consistent with our hypothesis. However, baseline EA discharge will include long ISIs evoking a large (non-depressed) AMPA-R component. We hypothesize that, at least for CLS and LS cells, baseline discharge can be weakly correlated because it is triggered by the AMPA-R component of the EPSP. Sensory stimulation, by shortening ISIs, causes depression of AMPA-R EPSPs; noise correlations are reduced because spiking is then evoked by membrane noise riding on slow NMDA-R EPSPs.

We hypothesize that ON (and likely OFF) cell discharge in the CMS and CLS maps, in response to low frequency input confined to their receptive fields, will be generated by intrinsic noise (blips). The response of cells with overlapping receptive fields will therefore be uncorrelated. This, in turn, will enable averaging the independent responses by downstream neurons and therefore enhance the detection and estimation of the weakest, e.g., prey signals. Clearly further experiments are required to verify these hypotheses.

Our results also point to a role for noise in signal encoding - facilitating encoding in a voltage-dependent manner. Blips are the main feature of this membrane noise and enable spiking where it would not otherwise occur. Noise-assisted signal encoding as in the stochastic resonance effect (Longtin, 1993; Gammaitoni et al., 1998; Hänggi, 2002) falls under the broader heading of stochastic facilitation (Longtin, 1993; McDonnell and Ward, 2011). It assumes that the stimulus evoked EPSPs are subthreshold, as expected

for weak stimuli, or generally stimuli that sit below threshold due to net bias inputs from the circuitry. For our study, where signals are slow and aperiodic, SR is referred to as aperiodic stochastic resonance (Collins et al., 1995). Noise-assisted stimulus encoding has been demonstrated *in vitro* in hippocampal cells with current injection (Stacey and Durand, 2001). Our study reveals that this effect is likely present here due to noisy blips arising near threshold. Due to the voltage-dependence of the rate of occurrence of these blips, and consequently of the noise variance (Figs. 7, 8C), the noise is amplified just where it is needed, namely, when subthreshold activity reaches spiking threshold. Thus not only does our study show that spikes are associated with noise blips and thus noise assists stimulus encoding at the second stage of a sensory system, it also relies on the voltage-dependence of this noise.

Let us put this result in a broader context. A modeling study (Chacron et al., 2000) predicted that EAs operate in the suprathreshold regime for baseline firing, meaning that firings would still occur in the absence of noise. The same goes for encoding of zero-mean amplitude modulations into a modulation of baseline activity. Thus noise in these receptors does not help the encoding of subthreshold stimuli, and SR is not at work; noise is nevertheless thought to help by linearizing the EA input-output firing rate function, smoothing over nonlinear phase locking effects (Knight, 1972).

Our results suggest that the next stage (ELL) is poised to detect any small modulations of baseline EA firing using noise. We cannot carry out the required classic experiment to prove that SR is at work, i.e. we cannot show that the input-output correlation of a pyramidal cell peaks for an intermediate noise level by adding and suppressing noise. The reason is that we cannot vary the noise level alone – at the very

least the noise level co-varies with the mean of the membrane potential, i.e. it is voltage-dependent. Nevertheless, the fact that the noise increases right at the limit of detection of the signal suggests that the noise-induced firing helps encode the signal. In fact, upward excursions of the signal will recruit more blips, with the result that the (stochastic) rate of firing is modulated by the signal.

Hence, post-synaptically to the EAs, it appears that noise helps the encoding process, in contrast to the EA level where the signal appears to modulate an already suprathreshold baseline firing pattern. It is also clear that too much noise at the second stage will degrade the encoding, as in the SR effect. It is tempting to further investigate whether this suprathreshold-followed-by-subthreshold encoding is a more general design principle of sensory systems, and whether an optimal noise level associated with a voltage-dependent stochastic resonance is at play here and in other systems.

The ISI decorrelation process supported mainly by the NMDA-R synaptic component appears to combine with noise-induced firing to ensure a sensitive encoding of naturalistic stimuli. The true statistics of the input spikes from multiple EAs to ON cells is not fully known, and the summed spike train may already have altered serial correlations compared to single EAs (Lindner, 2006). The interaction of the summed EA spike trains and postsynaptic dynamics remains a critical but challenging subject for future investigation.

Conclusions

A. The EA negative ISI correlations are not transmitted to successive EPSP peak amplitudes by the NMDA-R component of the EA to ON cell synapses. We hypothesize that the ISI correlations would otherwise be transmitted as variable amplitude peaks of the AMPA-R component and act as a high frequency noise source. This elimination of EPSP correlations is consistent with the theoretical optimal coding predictions of Nesse et al. (2010), which requires that the effective time scale of the post-synaptic response be similar to the EA adaptation time scale giving rise to the negative ISI correlations.

B. The response of CMS ON cells to the low frequency signals produced by, e.g. prey, is driven primarily by the dynamic balance of slow NMDA-R component of the EA-evoked EPSPs and disynaptic GABA-A mediated inhibition.

C. The evoked spiking response of ON cells is caused by intrinsic voltage-dependent noise riding on the NMDA-R component of the EA to ON cell EPSPs; this noise has renewal statistics. This has several important consequences: (1) The noise acts in a voltage-dependent manner to generate spikes near threshold; this suggests that stochastic resonance is at play to express weak or peri-threshold signals in ON cell spiking responses; (2) ON cell spiking is not phase locked to the EOD; (3) ON cell baseline discharge also has renewal statistics and is therefore ideally suited for inhomogeneous rate coding; (4) Neighboring ON cells with overlapping receptive fields therefore have uncorrelated spiking responses to, e.g., prey signals. Their outputs are therefore independent and can be effectively summed by their downstream midbrain target neurons.

Chapter 3: Discussion

The ability of neurons to encode and extract behaviorally relevant information from complex sensory signals remains a central area of study in sensory neuroscience. The weakly electric fish *Apteronotus leptorhynchus* continues to serve as a useful model organism for the study of sensory coding. The research presented in this thesis provides further insight into the cellular mechanisms that may be responsible for encoding prey-like sensory signals.

First, NMDA-R mediated temporal summation of EPSPs effectively eliminate electroreceptor afferent ISI correlations. The slow temporal kinetics of NMDA-R mediated currents balance the AMPA-R fast short-term depression and provide a mechanism for synaptic temporal decorrelation at the electroreceptor afferent ELL pyramidal cell synapse. We hypothesize that the AMPA-R induced negative amplitude correlations are a source of high frequency synaptic noise and that their removal by post-synaptic NMDA-R dynamics allows the peak membrane potential amplitudes to represent the stimulus and ultimately improve low frequency signal transmission.

Second, NMDA-R mediated temporal summation combined with GABA-A-R mediated disynaptic inhibition is required for the encoding and amplification of prey-like sensory signals. NMDA-R mediated temporal summation over many ISIs allows the pyramidal cell membrane potential to reconstruct low frequency sensory signals in the absence of network feedback. Experimental findings suggest that GABA-A plays a more active role than simply preventing NMDA-R saturation, and that an intricate balance between NMDA-R and GABA-A-R mediated currents is essential to encode prey signals. AMPA-R mediated EPSPs are crucial for the activation of NMDA-R currents, but do not

further contribute to encoding low frequency sensory signals. Post-synaptic AMPA-R mediated EPSPs are depressed during high frequency stimulation, during which NMDA-R mediated temporal summation depolarizes the pyramidal cell to near-threshold and ON-cell response is most likely to occur. Despite this ability of combined NMDA-R and GABA-A-R responses to accurately encode prey-like signals, the resulting membrane potential fluctuations are smooth in response to high frequency stimulation, during which robust ON cell responses are observed *in vivo*. A study by Chacron et al. (2007) demonstrated that spiking in ON cells is evoked by rapid membrane depolarizations, which suggests that an additional mechanism in combination with NMDA-R mediated temporal summation is responsible for evoking action potentials in ON cells. We therefore examined whether a previously described membrane noise in ELL pyramidal cells may evoke spiking when occurring on top of the smooth NMDA-R mediated depolarization.

Finally, experiments support an intrinsic voltage-dependent form of noise as the predominate source of spiking in ELL pyramidal neurons. ON cells respond to high frequency electroreceptor afferent input with small fluctuations in membrane potential (<2 mV) that are likely insufficient on their own to drive spiking; however, *in vivo* experiments suggest that these EPSPs are able to evoke a robust response (Mehaffey et al., 2008). We describe a voltage-dependent intrinsic noise with rapid rising slope that may drive pyramidal cells to spike when riding on smooth NMDA-R mediated depolarization and ultimately help encode sub-threshold sensory signals. These results are further supported by previous studies showing that ON cells are not phase locked to EOD (Krahe et al., 2008), and ON cells with overlapping receptive fields do not display

correlations to common input (Krahe et al., 2002).

The principles that operate in the ELL have also been noted in other sensory systems. Here, I discuss the contributions of AMPA, NMDA and GABA-A receptors to low-level signal processing in the visual and auditory system. I then review the mechanisms of noise generation at the cellular level, followed by a discussion of how noise may potentially benefit neuronal networks.

While AMPA receptors are commonly thought to be involved in evoking and transmitting action potentials between neurons as a result of their fast kinetics, NMDA receptors are more often linked to activity-dependent plasticity and long-term changes in neural circuitry. Nonetheless, NMDA receptors are found in sensory pathways and have been shown to be involved in sensory transmission. For example, NMDA receptors are found at multiple levels of the visual system, including in the retina (Fletcher et al., 2000), lateral geniculate nucleus, and throughout the visual cortex (Fox et al., 1990). Furthermore, the visual response in lagged thalamocortical relay cells of the LGN is mediated nearly entirely through NMDA receptors (Heggelund and Hartveit, 1990; Kwon et al., 1991), while excitatory input to non-lagged LGN cells are mediated primarily by AMPA receptors (Hartveit and Heggelund, 1990; Kielland and Heggelund, 2001). Lagged cells and non-lagged cells share a similar receptive field, however lagged cells respond to sensory stimuli with initial strong suppression followed by a more sustained firing, while non-lagged cells respond to similar stimuli with a brief high frequency burst followed by lower frequency sustained firing (Heggelund and Hartveit, 1990). Similar to ELL pyramidal cells, thalamocortical cells demonstrate strong AMPA receptor mediated depression at shorter ISIs (Kielland and Heggelund, 2001), with stimulation at

high enough frequencies (50 Hz) depressing AMPA-R response to such an extent that it is unable to generate spiking (Augustinaite and Heggelund, 2007). Despite the AMPA receptor depression during high frequency stimulation, the NMDA component of the EPSPs exhibit temporal summation to bring the membrane potential near threshold (Augustinaite and Heggelund, 2007). The authors suggest that the preservation of spike timing in non-lagged cells of LGN is the combined result of NMDA-R mediated temporal summation bringing the neurons to spike threshold at which time the small AMPA-R component is able to generate precisely timed spikes (Augustinaite and Heggelund, 2007). Conversely, lagged cells elicit spikes with more variable timing with reference to afferent input (Blitz and Regehr, 2003) at least in part through NMDA-receptors. The role of GABA-A receptor mediated disynaptic inhibition in thalamocortical cells of the dorsal LGN is far less understood. Inhibitory interneurons generate fast IPSPs that proceed EPSPs generated from retinal afferent spiking (Lindstro, 1982). It is speculated that GABA-A-R mediated inhibition may control the rate of depolarization induced by NMDA-R mediated temporal summation, and ultimately sculpt thalamocortical cell response through fast inhibition (Augustinaite and Heggelund, 2007).

Acoustic information is transmitted via the auditory nerve to several parallel pathways in the cochlear nucleus: pathways though the dorsal cochlear nucleus (DCN) and pathways through the ventral cochlear nucleus (VCN). Those through the DCN are thought to be responsible for the detection of spectral cues for localizing sound monaurally (Kanold and Young, 2001), while pathways through the VCN encode spectral and temporal information necessary for binaural localization and recognition of sound in the horizontal plane (Rhode and Smith, 1986). VCN cells demonstrate a tremendous

ability to phase lock their action potentials to auditory stimuli with a temporal precision on the range of 100 μsec (Oertel, 1999). These rapid and robust responses to acoustic stimuli in the VCN are a result of the rapid channel-gating kinetics of post-synaptic AMPA receptors (Raman and Trussell, 1992; Raman et al., 1994). NMDA receptors contribute only minimally in synaptic transmission in these same neurons (Isaacson and Walmsley, 1995). Conversely, subsets of cells within the DCN respond to acoustic stimuli with action potential responses that vary in timing over 100 msec (Parham and Kim, 1995). Presumably, the spike timing variability in these cells is mediated by the large NMDA-R component of their cochlear afferent synaptic input. The functional reason for this variability is not known. Overall, however, it seems that NMDA receptors contribute minimally, if at all, to synaptic transmission in cells transmitting precisely-timed signals in the cochlear nucleus.

Stochastic membrane fluctuations (noise) are a widely described phenomenon in the nervous system and are thought to be the primary determinant of behavioral variability that is observed under controlled conditions. Such variability is also seen at the cellular level, with repeated identical stimuli generating variability in spike timing across trials (Mainen and Sejnowski, 1995; van Steveninck et al., 1997). Many sources of neuronal noise have been described relating to the stochastic nature of biochemical processes that occur in neurons, for example the opening and closing of ion channels and the release, diffusion and fusion of neurotransmitters to synaptic receptors. While it is often assumed that the number of ion channels, synapses, and synaptic receptors essentially eliminate any significant randomness that may be generated by these individual stochastic elements, under certain conditions even small amounts of noise can

influence signal encoding. For example, small changes in membrane potential caused by random fluctuations in channel opening may be adequate to trigger spiking when neurons are near threshold (Strassberg and DeFelice, 1993). Furthermore, stochastic opening of a small number of channels in hippocampal neurons have been shown to be sufficient to trigger action potentials (Johansson and Arhem, 1994). Even noise in systems with low variability in spike response on the order of milliseconds or lower should be considered as potentially physiologically relevant, as neurons have been shown to be able to detect the coincident arrival of action potentials on similar timescales (Stuart and Häusser, 2001; Matsushita and Kawasaki, 2005).

The main sources of electric noise in individual neurons are typically a combination of channel noise and synaptic noise. Channel noise represents currents generated from the random opening and closing of voltage and ligand gated channels. Synaptic noise refers to the probabilistic release of neurotransmitter at the myriad of synapses made by presynaptic cells onto a neuron. The experiments conducted in this thesis suggest that intrinsic membrane properties, or channel noise, are responsible for the voltage-dependent noise in ELL pyramidal neurons. While the exact biophysical mechanism of this noise remains unknown, a previous study suggests that Na^+ channels are responsible (Mathieson and Maler, 1988). Neocortical pyramidal neurons have also shown similar voltage-dependent Na^+ channel noise that increases over the subthreshold voltage range (Jacobson et al., 2005). Further, a study of medial entorhinal cortex neurons demonstrated that stochastic gating of persistent Na^+ channels was necessary to account for membrane oscillations and spiking (White et al., 1998). In contrast, O'Donnell and van Rossum (2014) suggest that K^+ channels have a greater potential to

contribute towards membrane noise, but acknowledge that substantial channel noise can also arise from Na^+ channels. Both Na^+ and K^+ channels are found ubiquitously in the nervous system (Llinás, 1988).

While it is widely recognized that intrinsic noise limits the temporal accuracy of a neuronal output and many studies have focused on compensatory mechanisms by which it can be overcome, relatively few studies have focused on the computational advantages created by noise. Noise can enhance the ability of certain systems to detect and transmit weak signals, a form of stochastic resonance (Longtin, 1993; Gammaitoni et al., 1998; Hänggi, 2002). In the ELL, we show that voltage-dependent noisy blips are amplified at the sub- or peri-threshold level and convert the smooth synaptic responses of ON cells into spikes, ultimately assisting in encoding of weak sensory signals. Such endogenous noise-assisted signal detection has also been shown in hippocampal neurons (Stacey and Durand, 2001). Many systems depend on numerous EPSPs to be generated nearly simultaneously from often electronically distant areas of the neuron in order to evoke an action potential. Stochastic resonance may be a prominent feature of neurons, enabling these weak signals to be amplified and accounting for the stochastic nature of spiking in neurons throughout the nervous system.

Despite significant differences between the electric sense and the human senses of vision and audition, all of these senses are effectively able to detect weak signals and to estimate their intensity. I believe that the principles described in this thesis, namely slow excitation (NMDA) and dynamic inhibition (GABA-A) combined with signal decorrelation and amplification by membrane noise, may govern low level sensory processing and transmission across multiple sensory systems. The experiments in this

thesis further demonstrate the value of simple model systems in gaining insight into general principles that underlie complex processes in more advanced systems that are otherwise not amenable to study.

References

Augustinaite S, Heggelund P (2007) Changes in firing pattern of lateral geniculate neurons caused by membrane potential dependent modulation of retinal input through NMDA receptors. J Physiol 582:297-315.

Azouz R, Gray CM (2000) Dynamic spike threshold reveals a mechanism for synaptic coincidence detection in cortical neurons in vivo. Proc Natl Acad Sci U S A 97:8110-8115.

Azouz R, Gray CM (2003) Adaptive coincidence detection and dynamic gain control in visual cortical neurons in vivo. Neuron 37:513-523.

Bastian J (1981a) Electrolocation I. How the electroreceptors of Apteronotus Albifrons code for moving objects and other electrical stimuli. J Comp Physiol A 144:465-479.

Bastian J (1981b) Electrolocation II. The effects of moving objects and other electrical stimuli on the activities of two categories of posterior lateral line lobe cells in Apteronotus abffrons. J Comp Physiol A 144:481-494.

Bastian J (1996) Plasticity in an electrosensory system. I. General features of a dynamic sensory filter. J Neurophysiol 76:2483-2496.

Bastian J, Courtright J (1991) Morphological correlates of pyramidal cell adaptation rate in the electrosensory lateral line lobe of weakly electric fish. J Comp Physiol A 168:393-407.

Bastian J, Nguyenkim J (2001) Dendritic modulation of burst-like firing in sensory neurons. J Neurophysiol 85:10-22.

Bastian J, Courtright J, Crawford J (1993) Commissural neurons of the electrosensory lateral line lobe of Apteronotus leptorhynchus: morphological and physiological characteristics. J Comp Physiol A 173:257-274.

Bastian J, Chacron MJ, Maler L (2002) Receptive field organization determines pyramidal cell stimulus-encoding capability and spatial stimulus selectivity. J Neurosci 22:4577-4590.

Bastian J, Chacron MJ, Maler L (2004) Plastic and nonplastic pyramidal cells perform unique roles in a network capable of adaptive redundancy reduction. Neuron 41:767-779.

Benda J, Longtin A, Maler L (2005) Spike-frequency adaptation separates transient communication signals from background oscillations. J Neurosci 25:2312-2321.

Benda J, Longtin A, Maler L (2006) A synchronization-desynchronization code for natural communication signals. Neuron 52:347-358.

Bennett MVL (1971) Electroreception. Fish Physiol 5:493-574.

Bennett MVL, Sandri C, Akert K (1989) Fine structure of the tuberous electroreceptor of the high-frequency electric fish, Sternarchus albifrons (gymnotiformes). J Neurocytol 18:265-283.

Berman N, Dunn RJ, Maler L (2001) Function of NMDA receptors and persistent sodium channels in a feedback pathway of the electrosensory system. J Neurophysiol 86:1612-1621.

Berman NJ, Maler L (1998) Inhibition evoked from primary afferents in the electrosensory lateral line lobe of the weakly electric fish (Apteronotus leptorhynchus). J Neurophysiol 80:3173-3196.

Berman NJ, Maler L (1999) Neural architecture of the electrosensory lateral line lobe: adaptations for coincidence detection, a sensory searchlight and frequency-dependent adaptive filtering. J Exp Biol 202:1243-1253.

Berman NJ, Plant J, Turner RW, Maler L (1997) Excitatory amino acid receptors at a feedback pathway in the electrosensory system: implications for the searchlight hypothesis. J Neurophysiol 78:1869-1881.

Blitz DM, Regehr WG (2003) Retinogeniculate synaptic properties controlling spike number and timing in relay neurons. J Neurophysiol 90:2438-2450.

Bottai D, Dunn RJ, Ellis W, Maler L (1997) N‐methyl‐D‐aspartate receptor 1 mRNA distribution in the central nervous system of the weakly electric fish Apteronotus leptorhynchus. J Comp Neurol 389:65-80.

Calford MB, Aitkin LM (1983) Ascending projections to the medial geniculate body of the cat: evidence for multiple, parallel auditory pathways through thalamus. J Neurosci 3:2365-2380.

Carr CE, Maler L, Sas E (1982) Peripheral organization and central projections of the electrosensory nerves in gymnotiform fish. J Comp Neurol 211:139-153.

Carr CE, Maler L, Heiligenberg W, Sas E (1981) Laminar organization of the afferent and efferent systems of the torus semicircularis of gymnotiform fish: morphological substrates for parallel processing in the electrosensory system. J Comp Neurol 203:649-670.

Chacron MJ (2006) Nonlinear information processing in a model sensory system. J Neurophysiol 95:2933-2946.

Chacron MJ, Bastian J (2008) Population coding by electrosensory neurons. J Neurophysiol 99:1825-1835.

Chacron MJ, Longtin A, Maler L (2001) Negative interspike interval correlations increase the neuronal capacity for encoding time-dependent stimuli. J Neurosci 21:5328-5343.

Chacron MJ, Maler L, Bastian J (2005) Electroreceptor neuron dynamics shape information transmission. Nat Neurosci 8:673-678.

Chacron MJ, Lindner B, Longtin A (2007) Threshold fatigue and information transfer. J Comput Neurosci 23:301-311.

Chacron MJ, Longtin A, Maler L (2011) Efficient computation via sparse coding in electrosensory neural networks. Curr Opin Neurobiol 21:752-760.

Chacron MJ, Longtin A, St-Hilaire M, Maler L (2000) Suprathreshold stochastic firing dynamics with memory in P-type electroreceptors. Phys Rev Lett 85:1576-1579.

Chacron MJ, Doiron B, Maler L, Longtin A, Bastian J (2003) Non-classical receptive field mediates switch in a sensory neuron's frequency tuning. Nature 423:77-81.

Chen L, House JL, Krahe R, Nelson ME (2005) Modeling signal and background components of electrosensory scenes. J Comp Physiol A 191:331-345.

Clarke SE, Longtin A, Maler L (2014) A neural code for looming and receding motion is distributed over a population of electrosensory ON and OFF contrast cells. J Neurosci 34:5583-5594.

Clarke SE, Longtin A, Maler L (2015) A neural code for looming and receding motion is distributed over a population of electrosensory ON and OFF contrast cells. J Neurosci In press.

Clements JD, Lester RAJ, Tong G, Jahr CE, Westbrook GL (1992) The Time Course of Glutamate in the Synaptic Cleft. Science 258:1498-1501.

Collins JJ, Chow CC, Imhoff TT (1995) Aperiodic stochastic resonance in excitable systems. Phys Rev E Stat Phys Plasmas Fluids Relat Interdiscip Topics 52:R3321-R3324.

Deng Q, Rashid AJ, Fernandez FR, Turner RW, Maler L, Dunn RJ (2005) A C-terminal domain directs Kv3. 3 channels to dendrites. J Neurosci 25:11531-11541.

Dingledine R, Borges K, Bowie D, Traynelis SF (1999) The glutamate receptor ion channels. Pharmacol Rev 51:7-61.

Doiron B, Noonan L, Lemon N, Turner RW (2003) Persistent Na+ current modifies burst discharge by regulating conditional backpropagation of dendritic spikes. J Neurophysiol 89:324-337.

Dzubay JA, Jahr CE (1999) The concentration of synaptically released glutamate outside of the climbing fiber-Purkinje cell synaptic cleft. J Neurosci 19:5265-5274.

Engler G, Zupanc G (2001) Differential production of chirping behavior evoked by electrical stimulation of the weakly electric fish, Apteronotus leptorhynchus. J Comp Physiol A 187:747-756.

Felleman DJ, Van Essen DC (1991) Distributed hierarchical processing in the primate cerebral cortex. Cereb Cortex 1:1-47.

Fletcher EL, Hack I, Brandstätter JH, Wässle H (2000) Synaptic localization of NMDA receptor subunits in the rat retina. J Comp Neurol 420:98-112.

Fox K, Sato H, Daw N (1990) The effect of varying stimulus intensity on NMDA-receptor activity in cat visual cortex. J Neurophysiol 64:1413-1428.

Gammaitoni L, Hänggi P, Jung P, Marchesoni F (1998) Stochastic resonance. Rev Mod Phys 70:223.

Goense JB, Ratnam R (2003) Continuous detection of weak sensory signals in afferent spike trains: the role of anti-correlated interspike intervals in detection performance. J Comp Physiol A 189:741-759.

Goldman MS, Maldonado P, Abbott LF (2002) Redundancy reduction and sustained firing with stochastic depressing synapses. J Neurosci 22:584-591.

Gussin D, Benda J, Maler L (2007) Limits of linear rate coding of dynamic stimuli by electroreceptor afferents. J Neurophysiol 97:2917-2929.

Hagedorn M, Heiligenberg W (1985) Court and spark: electric signals in the courtship and mating of gymnotoid fish. Anim Behav 33:254-265.

Hänggi P (2002) Stochastic resonance in biology how noise can enhance detection of weak signals and help improve biological information processing. ChemPhysChem 3:285-290.

Hartveit E, Heggelund P (1990) Neurotransmitter receptors mediating excitatory input to cells in the cat lateral geniculate nucleus. II. Nonlagged cells. J Neurophysiol 63:1361-1372.

Harvey-Girard E, Maler L (2013) Dendritic SK channels convert NMDA-R-dependent LTD to burst timing-dependent plasticity. J Neurophysiol 110:2689-2703.

Harvey-Girard E, Dunn RJ, Maler L (2007) Regulated expression of N-methyl-D-aspartate receptors and associated proteins in teleost electrosensory system and telencephalon. J Comp Neurol 505:644-668.

Harvey-Girard E, Lewis J, Maler L (2010) Burst-induced anti-Hebbian depression acts through short-term synaptic dynamics to cancel redundant sensory signals. J Neurosci 30:6152-6169.

Heggelund P, Hartveit E (1990) Neurotransmitter receptors mediating excitatory input to cells in the cat lateral geniculate nucleus. I. Lagged cells. J Neurophysiol 63:1347-1360.

Heiligenberg W (1980) The jamming avoidance response in the weakly electric fishEigenmannia. Naturwissenschaften 67:499-507.

Heiligenberg W (1991) Neural nets in electric fish: MIT press Cambridge, MA.

Isaacson JS, Walmsley B (1995) Receptors underlying excitatory synaptic transmission in slices of the rat anteroventral cochlear nucleus. J Neurophysiol 73:964-973.

Jacobson GA, Diba K, Yaron-Jakoubovitch A, Oz Y, Koch C, Segev I, Yarom Y (2005) Subthreshold voltage noise of rat neocortical pyramidal neurones. J Physiol 564:145-160.

Johansson S, Arhem P (1994) Single-channel currents trigger action potentials in small cultured hippocampal neurons. Proc Natl Acad Sci U S A 91:1761-1765.

Kanold PO, Young ED (2001) Proprioceptive information from the pinna provides somatosensory input to cat dorsal cochlear nucleus. J Neurosci 21:7848-7858.

Khanbabaie R, Nesse WH, Longtin A, Maler L (2010) Kinetics of fast short-term depression are matched to spike train statistics to reduce noise. J Neurophysiol 103:3337-3348.

Khosravi-Hashemi N, Chacron MJ (2014) Motion processing across multiple topographic maps in the electrosensory system. Physiol Rep 2:e00253.

Kielland A, Heggelund P (2001) AMPA receptor properties at the synapse between retinal afferents and thalamocortical cells in the dorsal lateral geniculate nucleus of the rat. Neurosci Lett 316:59-62.

Kirschbaum F (1983) Myogenic electric organ precedes the neurogenic organ in apteronotid fish. Naturwissenschaften 70:205-207.

Knight BW (1972) Dynamics of encoding in a population of neurons. J Gen Physiol 59:734-766.

Knudsen EI (1974) Behavioral Thresholds to Electric Signals in High-Frequency Electric Fish. J Comp Physiol 91:333-353.

Krahe R, Maler L (2014) Neural maps in the electrosensory system of weakly electric fish. Curr Opin Neurobiol 24:13-21.

Krahe R, Bastian J, Chacron MJ (2008) Temporal processing across multiple topographic maps in the electrosensory system. J Neurophysiol 100:852-867.

Krahe R, Kreiman G, Gabbiani F, Koch C, Metzner W (2002) Stimulus encoding and feature extraction by multiple sensory neurons. J Neurosci 22:2374-2382.

Kwon YH, Esguerra M, Sur M (1991) NMDA and non-NMDA receptors mediate visual responses of neurons in the cat's lateral geniculate nucleus. J Neurophysiol 66:414-428.

Lannoo MJ, Lannoo SJ (1993) Why do electric fishes swim backwards? An hypothesis based on gymnotiform foraging behavior interpreted through sensory constraints. Environ Biol Fishes 36:157-165.

Lannoo MJ, Maler L, Tinner B (1989) Ganglion cell arrangement and axonal trajectories in the anterior lateral line nerve of the weakly electric fish Apteronotus leptorhynchus (Gymnotiformes). J Comp Neurol 280:331-342.

Lindner B (2006) Superposition of many independent spike trains is generally not a Poisson process. Phys Rev E Stat Nonlin Soft Matter Phys 73:022901.

Lindstro S (1982) Synaptic organization of inhibitory pathways to principal cells in the lateral geniculate nucleus of the cat. Brain Res 234:447-453.

Litwin-Kumar A, Chacron MJ, Doiron B (2012) The spatial structure of stimuli shapes the timescale of correlations in population spiking activity. PLoS Comput Biol 8:e1002667.

Llinás RR (1988) The intrinsic electrophysiological properties of mammalian neurons: insights into central nervous system function. Science 242:1654-1664.

Longtin A (1993) Stochastic Resonance in Neuron Models. J Stat Phys 70:309-327.

Ludtke N, Nelson ME (2006) Short-term synaptic plasticity can enhance weak signal detectability in nonrenewal spike trains. Neural Comput 18:2879-2916.

Maciver MA, Sharabash NM, Nelson ME (2001) Prey-capture behavior in gymnotid electric fish: motion analysis and effects of water conductivity. J Exp Biol 204:543-557.

Mainen ZF, Sejnowski TJ (1995) Reliability of spike timing in neocortical neurons. Science 268:1503-1506.

Maler L (1979) The posterior lateral line lobe of certain gymnotoid fish: quantitative light microscopy. J Comp Neurol 183:323-363.

Maler L (2009a) Receptive field organization across multiple electrosensory maps. I. Columnar organization and estimation of receptive field size. J Comp Neurol 516:376-393.

Maler L (2009b) Receptive field organization across multiple electrosensory maps. II. Computational analysis of the effects of receptive field size on prey localization. J Comp Neurol 516:394-422.

Maler L, Mugnaini E (1994) Correlating gamma-aminobutyric acidergic circuits and sensory function in the electrosensory lateral line lobe of a gymnotiform fish. J Comp Neurol 345:224-252.

Maler L, Sas EK, Rogers J (1981) The cytology of the posterior lateral line lobe of high-frequency weakly electric fish (Gymnotidae): dendritic differentiation and synaptic specificity in a simple cortex. J Comp Neurol 195:87-139.

Markham MR (2013) Electrocyte physiology: 50 years later. J Exp Biol 216:2451-2458.

Marsat G, Proville RD, Maler L (2009) Transient signals trigger synchronous bursts in an identified population of neurons. J Neurophysiol 102:714-723.

Marsat G, Longtin A, Maler L (2012) Cellular and circuit properties supporting different sensory coding strategies in electric fish and other systems. Curr Opin Neurobiol 22:686-692.

Mathieson WB, Maler L (1988) Morphological and electrophysiological properties of a novel in vitro preparation: the electrosensory lateral line lobe brain slice. J Comp Physiol A 163:489-506.

Matsubara J, Heiligenberg W (1978) How well do electric fish electrolocate under jamming? J Comp Physiol A 125:285-290.

Matsushita A, Kawasaki M (2005) Neuronal sensitivity to microsecond time disparities in the electrosensory system of Gymnarchus niloticus. J Neurosci 25:11424-11432.

McDonnell MD, Ward LM (2011) The benefits of noise in neural systems: bridging theory and experiment. Nat Rev Neurosci 12:415-U489.

Mehaffey WH, Maler L, Turner RW (2008) Intrinsic frequency tuning in ELL pyramidal cells varies across electrosensory maps. J Neurophysiol 99:2641-2655.

Merigan WH, Maunsell JHR (1993) How parallel are the primate visual pathways? Annu Rev Neurosci 16:369-402.

Metzner W (1999) Why are there so many sensory brain maps? Cell Mol Life Sci 56:1-4.

Mountcastle VB (1997) The columnar organization of the neocortex. Brain 120:701-722.

Nelson ME, Maciver MA (1999) Prey capture in the weakly electric fish Apteronotus albifrons: sensory acquisition strategies and electrosensory consequences. J Exp Biol 202:1195-1203.

Nelson ME, Xu Z, Payne JR (1997) Characterization and modeling of P-type electrosensory afferent responses to amplitude modulations in a wave-type electric fish. J Comp Physiol A 181:532-544.

Nesse WH, Maler L, Longtin A (2010) Biophysical information representation in temporally correlated spike trains. Proc Natl Acad Sci U S A 107:21973-21978.

O'Donnell C, van Rossum MCW (2014) Systematic analysis of the contributions of stochastic voltage gated channels to neuronal noise. Front Comput Neurosci 8.

Oertel D (1999) The role of timing in the brain stem auditory nuclei of vertebrates. Annu Rev Physiol 61:497-519.

Parham K, Kim DO (1995) Spontaneous and sound-evoked discharge characteristics of complex-spiking neurons in the dorsal cochlear nucleus of the unanesthetized decerebrate cat. J Neurophysiol 73:550-561.

Pozzorini C, Naud R, Mensi S, Gerstner W (2013) Temporal whitening by power-law adaptation in neocortical neurons. Nat Neurosci 16:942-U216.

Raman IM, Trussell LO (1992) The kinetics of the response to glutamate and kainate in neurons of the avian cochlear nucleus. Neuron 9:173-186.

Raman IM, Zhang S, Trussell LO (1994) Pathway-specific variants of AMPA receptors and their contribution to neuronal signaling. J Neurosci 14:4998-5010.

Rasnow B (1996) The effects of simple objects on the electric field of Apteronotus. J Comp Physiol A 178:397-411.

Ratnam R, Nelson ME (2000) Nonrenewal statistics of electrosensory afferent spike trains: implications for the detection of weak sensory signals. J Neurosci 20:6672-6683.

Rauschecker JP, Tian B, Pons T, Mishkin M (1997) Serial and parallel processing in rhesus monkey auditory cortex. J Comp Neurol 382:89-103.

Rhode WS, Smith PH (1986) Encoding timing and intensity in the ventral cochlear nucleus of the cat. J Neurophysiol 56:261-286.

Saunders J, Bastian J (1984) The physiology and morphology of two types of electrosensory neurons in the weakly electric fishApteronotus leptorhynchus. J Comp Physiol A 154:199-209.

Schwalger T, Droste F, Lindner B (2015) Statistical structure of neural spiking under non-Poissonian or other non-white stimulation. J Comput Neurosci:1-23.

Shumway CA (1989) Multiple electrosensory maps in the medulla of weakly electric gymnotiform fish. I. Physiological differences. J Neurosci 9:4388-4399.

Stacey WC, Durand DM (2001) Synaptic noise improves detection of subthreshold signals in hippocampal CA1 neurons. J Neurophysiol 86:1104-1112.

Strassberg AF, DeFelice LJ (1993) Limitations of the Hodgkin-Huxley formalism: Effects of single channel kinetics on transmembrane voltage dynamics. Neural Comput 5:843-855.

Stuart GJ, Häusser M (2001) Dendritic coincidence detection of EPSPs and action potentials. Nat Neurosci 4:63-71.

Turner RW, Maler L, Deerinck T, Levinson SR, Ellisman MH (1994) TTX-sensitive dendritic sodium channels underlie oscillatory discharge in a vertebrate sensory neuron. J Neurosci 14:6453-6471.

van Steveninck RRdR, Lewen GD, Strong SP, Koberle R, Bialek W (1997) Reproducibility and variability in neural spike trains. Science 275:1805-1808.

Wang DL, Maler L (1994) The Immunocytochemical Localization of Glutamate in the Electrosensory System of the Gymnotiform Fish, Apteronotus-Leptorhynchus. Brain Res 653:215-222.

Wessel R, Koch C, Gabbiani F (1996) Coding of time-varying electric field amplitude modulations in a wave-type electric fish. J Neurophysiol 75:2280-2293.

White JA, Klink R, Alonso A, Kay AR (1998) Noise from voltage-gated ion channels may influence neuronal dynamics in the entorhinal cortex. J Neurophysiol 80:262-269.

Young ED (1998) Parallel processing in the nervous system: evidence from sensory maps. Proc Natl Acad Sci U S A 95:933-934.

Young ED, Davis KA (2002) Circuitry and function of the dorsal cochlear nucleus. In: Integrative functions in the mammalian auditory pathway, pp 160-206: Springer.